Zigzag and Breakup Instabilities of Stripes and Rings in the Two-Dimensional Gray-Scott Model

Theodore Kolokolnikov, Michael J. Ward, and Juncheng Wei

Abstract

Two different types of instabilities of equilibrium stripe and ring solutions to a singularly perturbed Gray-Scott model in a two-dimensional domain are studied in the limit of a small diffusivity ε of one of the two components of the reaction. An equilibrium stripe solution is obtained when the singularly perturbed component of the reaction concentrates along the mid-line of a rectangular domain. An equilibrium ring solution occurs when this component concentrates on some circle that lies concentrically within a circular cylindrical domain. These equilibrium stripe and ring solutions are constructed asymptotically in the limit $\varepsilon \to 0$, and the spectrum of the linearization with respect to transverse instabilities is analyzed. The first type of instability, which is associated with the eigenvalues of the linearization that are asymptotically small as $\varepsilon \to 0$, leads to the formation of zigzag patterns. The second type of instability, which is associated with eigenvalues that are $O(1)$ as $\varepsilon \to 0$, leads to the breakup of a stripe or a ring into spots. For both the stripe and the ring, a combination of asymptotic and numerical methods are used to to determine precise instability bands for both types of instabilities. The instability bands are found to depend on the relative magnitude, with respect to ε, of a non-dimensional feed-rate parameter A that appears in the coefficients of the non-dimensional Gray-Scott model. Instabilities occurring in both the high feed-rate regime, where $A = O(1)$, and the intermediate feed-rate regime where $O(\varepsilon^{1/2}) \ll A \ll 1$ are studied. The analysis is supplemented by full numerical simulations illustrating these instabilities.

1 Introduction

The Gray-Scott system [8], [9] models an irreversible reaction involving two reactants in a gel reactor, where the reactor is maintained in contact with a reservoir of one of the two chemicals in the reaction. In dimensionless variables, this system can be written as

$$V_T = D_v \Delta V - (F+k)V + UV^2 \,, \qquad X \text{ in } \Omega \,, \quad T > 0 \,, \tag{1.1a}$$

$$U_T = D_u U_{XX} + F(1-U) - UV^2 \,, \qquad X \text{ in } \Omega \,, \quad T > 0 \,, \tag{1.1b}$$

$$\partial_n U = \partial_n V = 0 \,, \qquad X \text{ on } \partial\Omega \,. \tag{1.1c}$$

Here the unknowns $U(X,T)$ and $V(X,T)$ represent the concentrations of the two biochemicals; D_U, D_V are the diffusion coefficients of U and V, respectively; X is the space variable in R^2; F denotes the rate at which U is fed from the reservoir into the reactor, k is a reaction-time constant, and ∂_n represents the outward normal derivative.

This model is known to have a rich solution structure for various parameter ranges. In two dimensions, spots, rings, stripes, traveling waves, self-replication, oscillating spikes, and spatio-temporal chaos have been observed. See [8], [9], [16], [17] for experimental work. For numerical and analytical results, see for instance [4], [5], [12], [20], [21], [22], [23], [24], [25], [26], [27], [28], [30], [31], and [32].

For our analysis it is convenient to first transform (1.1) into a a different non-dimensional form as was done in [20] (see also [13], [14], and [15]). We introduce

$$\varepsilon^2 = \frac{D_V F}{D_U(F+k)}\,, \qquad A = \frac{\sqrt{F}}{F+k}\,, \qquad \tau = \frac{F+k}{F}\,,$$

$$X = \sqrt{\frac{D_U}{F}}x\,, \qquad T = \frac{t}{F+k}\,, \qquad V(X,T) = \sqrt{F}v(x,t)\,, \qquad U(X,T) = u(x,t)\,.$$

In terms of these new variables, (1.1) becomes

$$v_t = \varepsilon^2 \Delta v - v + Auv^2\,, \qquad x \text{ in } \Omega\,, \quad t > 0\,, \tag{1.2a}$$

$$\tau u_t = \Delta u + (1-u) - uv^2 \qquad x \text{ in } \Omega\,, \quad t > 0\,, \tag{1.2b}$$

$$\partial_n u = \partial_n v = 0\,, \qquad x \text{ on } \partial\Omega\,. \tag{1.2c}$$

The goal of this paper is to study the stability as $\varepsilon \to 0$ of equilibrium stripe and ring solutions to (1.2) in a two-dimensional domain. An equilibrium stripe solution is obtained when v concentrates along the mid-line of a rectangular domain. Alternatively, an equilibrium ring solution occurs when v concentrates on some circle of radius ρ_0 that lies concentrically within a circular cylindrical domain of radius R. Accordingly, we will assume that Ω is either a rectangle or a disk (we also allow for an infinite rectangle or disk). Throughout this paper we will assume that $\varepsilon \ll 1$ and $\tau = O(1)$ as $\varepsilon \to 0$.

In recent works [15] and [19], the existence and stability of equilibrium ring solutions has been studied in what we shall call the *low feed-rate regime* characterized by $A = O(\varepsilon^{1/2})$. In addition, the existence and stability of spike solutions in the low feed-rate regime in a one-dimensional domain has been studied in [14]. For ring solutions in the low feed-rate regime it was shown in [15] that such a solution is always unstable with respect to spatial perturbations in v of the form $\cos(m\theta)\phi$, where ϕ is an even function near the ring, for some wide band of modes m. More precisely, it was shown in [15] that there exists values $m_1 = O(1)$ and $m_2 = O(\varepsilon^{-1})$, such that all modes m in the range

$m_1 \leq m \leq m_2$ are unstable, while all other modes are stable. Furthermore, it was also shown that m_1 increases as A is increased. Such an instability leads to a breakup of the ring into m spots. We shall therefore call it a breakup instability.

The precise goal of this paper is to study zigzag and breakup instabilities of rings and stripes in the regime $A \gg O(\varepsilon^{1/2})$. We will consider two important subcases:

$$\textit{Intermediate regime:} \quad O(\varepsilon^{1/2}) \ll A \ll O(1)\,; \qquad \textit{High feed-rate regime:} \quad A = O(1)\,.$$

The stability properties of rings and stripes in the intermediate and high feed-rate regimes are found to be very different from that of the low feed-rate regime. We shall consider two different types of instabilities. The first instability is associated with eigenvalues of the linearization that tend to zero as $\varepsilon \to 0$. These eigenvalues are referred to as the small eigenvalues. The corresponding eigenfunctions for both u and v are, locally, odd functions near the stripe or the ring. This type of instability leads to the formation of zigzag patterns such as shown below in Fig. 7. The second type of instability is associated with eigenvalues of the linearization that are $O(1)$ as $\varepsilon \to 0$. These eigenvalues are referred to as the large eigenvalues. The corresponding eigenfunctions for both u and v are, locally, even functions near the stripe or the ring. This type of instability is found to lead to the breakup of the ring or stripe into spots, such as shown below in Fig. 9. Using a combination of asymptotic and numerical methods, we give precise results for the occurrence of both types of instabilities for equilibrium stripe and ring solutions in both the intermediate and the high feed-rate regimes.

For zigzag instabilities, we show that there exists a band of unstable modes, for both the stripe and the ring, in the high feed-rate and intermediate regimes. More specifically, in the high feed-rate regime, we show that all unstable zigzag modes m satisfy $m_b \leq m \leq \varepsilon^{-1} m_u$ for some $O(1)$ thresholds m_b and m_u. The key results for zigzag instabilities of stripes and rings are given in Proposition 5 and Proposition 11, respectively. In the intermediate regime, we can calculate m_u asymptotically for a stripe. The existence of zigzag instabilities for the Gray-Scott model was first suggested by the numerical computations in [19]. However, no prior analysis of this type of instability for the Gray-Scott model has been performed. Our method to study zigzag instabilities is similar to the method developed in [13] for the analysis of small eigenvalues of the Gray-Scott model in one spatial dimension.

For breakup instabilities of stripes and rings, we use a combination of asymptotic and numerical methods for the high feed-rate regime to show that the unstable modes m are all within the band $m_l < \varepsilon m < m_u$ for some $O(1)$ thresholds m_l and m_u. Therefore, all of the unstable modes are of the order $m = O(\varepsilon^{-1})$. In the intermediate regime, we can estimate m_u and m_l analytically, and we show that $m_l = O(\delta^2)$, when $A = O(\delta)$, with $O(\varepsilon^{1/2}) \ll \delta \ll O(1)$. Precise results for breakup instabilities of stripes and rings are given in Propositions 7 and Proposition 12, respectively. In Conjecture 2.1 of

[15] it was anticipated that a ring may be stable if $A = O(1)$. Our results show that this conjecture is not true, as there always exists an unstable band of modes m with $m = O(\varepsilon^{-1})$.

There have been other studies of zigzag instabilities for related systems. In [10] a phase equation was derived to analyze Eckhaus and zigzag instabilities of periodic solutions of the Fitzhugh-Nagumo equation on the infinite line. In [33], labyrinthine patterns generated through either a transverse instability of a stripe or the nucleation of a stripe have been observed experimentally in a periodically forced BZ reaction. These patterns were then modeled theoretically using a complex Ginzburg-Landau equation. Zigzag instabilities and labyrinthine patterns were computed numerically in [7] using a contour dynamics approach for a Fitzhugh-Nagumo system. In [11] zigzag instabilities of a stripe in an unbounded domain were studied for a Fitzugh-Nagumo system using an amplitude equation approach, which is based on the underlying symmetries of the problem. Although this approach gives a weakly nonlinear theory, in [11] the coefficients in the normal form were not related to the coefficients in the underlying PDE. In contrast, our approach to analyze zigzag instabilities of stripes and rings relies heavily on the singular perturbation character of these solutions together with an asymptotic or numerical analyses of the underlying eigenvalue problems of the linearization. Although our analysis determines the onset of the instabilities in terms of the parameters in the PDE, it does not provide a weakly nonlinear theory for their development.

The outline of this paper is as follows. In §2 we construct an equilibrium stripe solution in the intermediate and high feed-rate regimes. In §3 we derive a main result, which characterizes the stability of a stripe with respect to zigzag instabilities. In §4 we study the breakup instability of an equilibrium stripe. Analogous results for zigzag and breakup instabilities of an equilibrium ring solution are derived in §5. Some numerical simulations are given in §6. A brief discussion is given in §7.

2 Asymptotic Construction of a Stripe Equilibrium

In the limit $\varepsilon \to 0$, we construct a one-stripe equilibrium solution to (1.2) in a rectangular domain of width $2l$ and of height d :

$$\Omega = [-l, l] \times [0, d] \,.$$

Since equilibrium stripes are inherently one-dimensional, the analysis is essentially the same as was done in [13] for the one-dimensional Gray-Scott model. A brief synopsis of this analysis is included here for the convenience of the reader.

In the high feed-rate regime where $A = O(1)$, we seek an inner solution near the center of the spike in the form (cf. [13])

$$v = \frac{V}{\varepsilon}\,, \qquad u = \frac{\varepsilon U}{A}\,, \qquad y = \frac{x_1}{\varepsilon}\,, \tag{2.1}$$

where both V and U are $O(1)$, and $x_1 \in [-l, l]$ is the first component of $x = (x_1, x_2)$. Substituting (2.1) into the steady-state problem for (1.2), we obtain that

$$V'' - V + V^2 U = 0\,, \tag{2.2a}$$

$$U'' - \varepsilon^2 U + A\varepsilon - V^2 U = 0\,. \tag{2.2b}$$

Therefore, we expand V and U as

$$V = V_0(y) + A\varepsilon V_1(y) + \cdots\,, \qquad U = U_0(y) + A\varepsilon U_1(y) + \cdots\,. \tag{2.3}$$

Substituting (2.3) into (2.2), and collecting powers of εA, we obtain on $-\infty < y < \infty$ that

$$V_0'' - V_0 + V_0^2 U_0 = 0\,, \tag{2.4a}$$

$$U_0'' - V_0^2 U_0 = 0\,, \tag{2.4b}$$

and

$$V_1'' - V_1 + 2V_0 U_0 V_1 + V_0^2 U_1 = 0\,, \tag{2.5a}$$

$$U_1'' + 1 - 2V_0 U_0 V_1 - V_0^2 U_1 = 0\,. \tag{2.5b}$$

The asymptotic boundary conditions for V_j are that $V_j \to 0$ as $|y| \to \infty$ for $j = 0, 1$. The asymptotic boundary conditions for U_j are determined upon matching to the outer solution.

Next, we consider the outer region. Since v is exponentially small in this region, we need only analyze u. To determine the effect of the inner solution on the outer problem for u, we first use the inner solution to calculate uv^2 in the sense of distributions. A simple calculation (cf. [13]) shows that

$$uv^2 \to C_0 \delta(x_1) + \varepsilon C_1 \delta(x_1) + \cdots\,, \qquad C_0 = \frac{1}{A}\int_{-\infty}^{\infty} U_0 V_0^2\, dy\,, \qquad C_1 = \int_{-\infty}^{\infty} \left(2U_0 V_0 V_1 + V_0^2 U_1\right)\, dy\,. \tag{2.6}$$

Substituting (2.6) into (1.2), we obtain the outer problem for u

$$u_{x_1 x_1} + (1-u) = C_0 \delta(x_1) + \varepsilon C_1 \delta(x_1) + \cdots\,, \quad -l < x_1 < l\,; \qquad u_{x_1}(\pm l) = 0\,. \tag{2.7}$$

Therefore, we expand the outer solution for u as $u = u_0 + \varepsilon u_1 + \cdots$. In this way, we obtain the two-term expansion

$$u = 1 - C_0 G_l(x_1) - \varepsilon C_1 G_l(x_1) + \cdots\,, \tag{2.8}$$

where $G_l(x_1)$ is the Green's function on $-l < x_1 < l$ satisfying

$$G_{lx_1x_1} - G_l = -\delta(x_1)\,, \quad -l < x_1 < l\,; \qquad G_{lx_1}(\pm l; 0) = 0\,. \tag{2.9}$$

A simple calculation gives

$$G_l(x_1) = \frac{\cosh\left[(l - |x_1|)\right]}{2\sinh(l)}\,. \tag{2.10}$$

To match the inner and outer expansions for u we require that

$$\frac{\varepsilon}{A}\left(U_0(y) + A\varepsilon U_1(y) + \cdots\right) \sim 1 - C_0 G_l(\varepsilon y) - \varepsilon C_1 G_l(\varepsilon y) + \cdots\,. \tag{2.11}$$

This matching condition yields that $1 - C_0 G_l(0) = 0$, and $U_0(y) \sim -AC_0 G_{lx_1}(0^{\pm})y$ as $y \to \pm\infty$. By calculating $G_l(0)$, $G_{lx_1}(0^{\pm})$ from (2.10), we obtain that $C_0 = 2\tanh(l)$, and

$$U_0 \sim B|y|\,, \quad \text{as} \quad |y| \to \infty\,, \qquad B \equiv \frac{C_0 A}{2} = A\tanh(l)\,. \tag{2.12}$$

In terms of the solution to (2.4) with the asymptotic boundary condition (2.12), there is a constant E, which depends on B, such that

$$U_0 - B|y| \to E\,, \qquad \text{as} \quad |y| \to \infty\,. \tag{2.13}$$

Substituting this expression into the matching condition (2.11), and calculating $G_l(0)$, $G_{lx_1}(0^{\pm})$, and $G_{lx_1x_1}(0)$, we obtain that $C_1 = -2EA^{-1}\tanh(l)$, together with the asymptotic boundary condition

$$U_1 \sim -\frac{y^2}{2} - \frac{E}{B}\tanh^2(l)|y|\,, \quad \text{as} \quad |y| \to \infty\,. \tag{2.14}$$

The problem for U_1, V_1 is then (2.5) together with $V_1 \to 0$ as $|y| \to \infty$ and (2.14) for U_1.

We label the *core problem* as (2.4) with the asymptotic boundary condition (2.12) and $V_0(\pm\infty) = 0$. We look for an even solution to this problem. In [13] (see also [20]), it was shown numerically that a one-bump solution to this core problem on $0 < y < \infty$, with $V_0'(0) = U_0'(0) = 0$, $V_0(\infty) = 0$, $U_0'(\infty) = B$, exists only for $B < 1.347$. To obtain this result it is convenient to introduce the parameter γ defined by

$$\gamma = V_0(0)U_0(0)\,. \tag{2.15}$$

In [13] it was shown that $0 \leq \gamma \leq \frac{3}{2}$. For each value of γ on this range a corresponding numerical value of B can be computed. The resulting plot is shown in Fig. 1. This graph has a fold point at $\gamma = 1.02$, where $B = 1.347$. We refer to the range $1.02 < \gamma < 1.5$ and $0 < \gamma < 1.02$ as the *primary* and *secondary* solution branches, respectively. The asymptotic construction of a one-stripe equilibrium solution to (1.2) is summarized as follows:

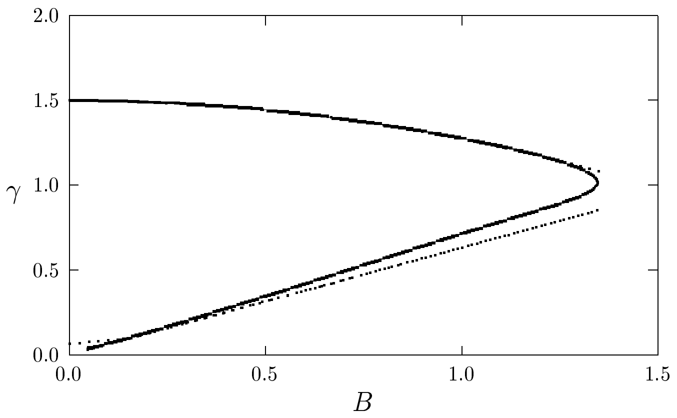

Figure 1: The graph of $\gamma = V_0(0)U_0(0)$ versus $B = U_0'(\infty)$. The fold point occurs at $\gamma = 1.02$, $B = 1.347$. The dashed curves represent asymptotic approximations to the curve at the two extremities as derived in [13]. The top branch is called the primary branch.

Proposition 1 *Let $\Omega = [-l, l] \times [0, d]$, and define B by*

$$B = A \tanh l \,. \tag{2.16}$$

Suppose that $A = O(1)$ and $B < 1.347$. Then, along the primary branch of the γ versus B curve, there exists a stripe equilibrium solution to (1.2) of the form

$$v_e \sim \frac{1}{\varepsilon}\left(V_0(y) + \varepsilon V_1(y) + \cdots\right), \qquad u_e \sim \frac{\varepsilon}{A}\left(U_0(y) + \varepsilon U_1(y) + \cdots\right), \qquad y = \varepsilon^{-1} x_1 \,, \tag{2.17}$$

where $V_0(y)$, $U_0(y)$ are even solutions to (2.4) subject to the boundary conditions

$$V_0'(0) = U_0'(0) = 0 \,, \qquad V_0(\infty) = 0 \,, \qquad U_0'(\infty) = B \,. \tag{2.18}$$

In the outer region, v_e is exponentially small, and the leading-order approximation to u_e is

$$u_e \sim 1 - \tanh l \left(\frac{\cosh(l - |x_1|)}{\sinh(l)}\right) + O(\varepsilon) \,. \tag{2.19}$$

In general, the core problem (2.4) and (2.18) must be solved numerically. However, when B is small, an asymptotic solution of the core problem can be obtained for both extremities of the γ versus B curve. At the extremity of the primary solution branch where $\gamma \to 3/2$ from below, an asymptotic solution to the core problem can be constructed as in [13]. This construction, which is summarized in the next result, shows the merging of the high feed-rate solution where $A = O(1)$ to the intermediate regime solution where $O(\varepsilon^{1/2}) \ll A \ll O(1)$.

Proposition 2 *([13], Proposition 4.1): In the intermediate regime we have*

$$B = 3\delta \quad \text{with} \quad O(\varepsilon^{1/2}) \ll \delta \ll O(1) \,. \tag{2.20}$$

In this limit, the core problem (2.4) with boundary conditions (2.18) admits the limiting stripe solution

$$V_0(y) \sim \delta \left(w(y) + \delta^2 v_1(y) + \cdots \right) \,, \qquad U_0(y) \sim \delta^{-1} \left(1 + \delta^2 u_1(y) + \cdots \right) \,, \tag{2.21}$$

where $w(y) = \frac{3}{2} \text{sech}^2 \left(y/2 \right)$ is the unique solution to

$$w'' - w + w^2 = 0 \qquad w'(0) = 0 \,, \quad w(0) > 0 \,, \quad w \to 0 \ \text{as} \ |y| \to \infty \,. \tag{2.22}$$

The correction u_1 satisfies

$$u_1'' = w^2 \,; \quad u_1'(0) = 0 \,, \quad u_1(0) = 0 \,, \tag{2.23}$$

and v_1 satisfies

$$v_1'' - v_1 + 2wv_1 = -w^2 u_1 \,, \quad v_1'(0) = 0 \,, \quad v_1 \to 0 \ \text{as} \ |y| \to \infty \,. \tag{2.24}$$

The corresponding local behavior of the γ versus B curve is $\gamma \equiv U_0(0)V_0(0) \sim \frac{3}{2} - 11B^2/48$.

A similar asymptotic construction can be done to calculate the local behavior of the γ versus B curve valid for $\gamma \to 0^+$. This latter result, which is not needed in the analysis below, is given in Proposition 4.2 of [13]. In Fig. 1 the dashed lines correspond to the two local behaviors of the γ versus B curve for $\gamma \to 0^+$ and $\gamma \to (3/2)^-$.

3 Zigzag Instabilities of a Stripe

In this section we study zigzag instabilities of the stripe equilibrium solutions constructed in §2 along the primary solution branch of the γ versus B curve. As before, we assume that our domain is a rectangle with $\Omega = [-l, l] \times [0, d]$. To see how zigzag instabilities can occur, we first consider a general reaction-diffusion model of the form

$$u_t = \varepsilon^2 \Delta u - F(u), \quad x \in \Omega,$$
$$\partial_n u = 0, \quad x \in \partial\Omega,$$

where u may have multiple components. Suppose that $u_0(x_1)$ is the (one-dimensional) solution to the equilibrium problem:

$$\varepsilon^2 \Delta u_0 = F(u_0).$$

If we linearize around this equilibrium solution by writing

$$u = u_0 + e^{\lambda t} \cos(m x_2) \Psi(x_1)\,,$$

we then obtain that

$$(\lambda + \varepsilon^2 m^2)\Psi = \varepsilon^2 \Psi'' - \nabla F(u_0) \cdot \Psi, \quad \text{with} \quad \Psi(\pm l) = 0\,.$$

When $l = \infty$, this equation is satisfied with $\lambda + \varepsilon^2 m^2 = 0, \Psi = C u_0'$. Therefore, it appears that $\lambda < 0$ when $m > 0$. However, if l is finite then $u_0'(l)$ may still be small, but not identically zero. This introduces a small correction to the eigenvalue, and may have a destabilizing effect on some of the modes m. The corresponding perturbation then has the form:

$$u = u_0(x_1) + c e^{\lambda t} \cos(m x_2) u_0'(x_1) \sim u_0 \left[x_1 + c e^{\lambda t} \cos(m x_2)\right]\,,$$

where c is some small constant. Clearly, instabilities in the location of the center of the stripe occur when $\mathrm{Re}(\lambda) > 0$. This is a brief description of the mechanism for the existence of zigzag instabilities.

We now give a detailed analysis of zigzag instabilities of stripe equilibria for the Gray-Scott model. Let v_e, u_e be the equilibrium stripe solution constructed in §2. We introduce a perturbation around this equilibrium state in the form

$$v = v_e + e^{\lambda t} e^{i m x_2} \phi\,, \qquad u = u_e + e^{\lambda t} e^{i m x_2} \eta\,, \qquad . \tag{3.1}$$

where $\phi \ll 1$ and $\eta \ll 1$. In order to satisfy the homogeneous Neumann conditions on the boundaries $x_2 = 0$ and $x_2 = d$ of Ω, we require that

$$m = \frac{k\pi}{d}\,, \tag{3.2}$$

where k is a non-negative integer. In the analysis below we will treat m as a continuous variable. The band of instability with respect to m that we will determine in the analysis can be mapped to a band of instability with respect to the integer k using (3.2).

Substituting (3.1) into (1.2), we obtain the following eigenvalue problem on $-l < x_1 < l$:

$$\lambda\phi = \varepsilon^2 \phi_{x_1 x_1} - \varepsilon^2 m^2 \phi - \phi + 2A u_e v_e \phi + A v_e^2 \eta\,, \tag{3.3a}$$

$$\tau\lambda\eta = \eta_{x_1 x_1} - m^2 \eta - \eta - 2 u_e v_e \phi - v_e^2 \eta\,. \tag{3.3b}$$

We will study this problem in the inner region where $y = \varepsilon^{-1}x_1 = O(1)$, and in the outer region defined away from an $O(\varepsilon)$ region near $x_1 = 0$.

In the inner region, the equilibrium solution is given by (2.17). Therefore, in this region we write

$$u_e = \frac{\varepsilon}{A}U\,, \quad v_e = \frac{V}{\varepsilon}\,, \quad \phi = \frac{1}{\varepsilon}\Phi\,, \quad \eta = \frac{\varepsilon}{A}N\,, \quad y = \varepsilon^{-1}x_1\,. \tag{3.4}$$

With these inner variables, (3.3) is transformed to the following eigenvalue problem on $-\infty < y < \infty$:

$$\lambda\Phi = \Phi'' - m^2\varepsilon^2\Phi - \Phi + V^2N + 2VU\Phi\,, \tag{3.5a}$$

$$\tau\varepsilon^2\lambda N = N'' - m^2\varepsilon^2 N - \varepsilon^2 N - V^2N - 2VU\Phi\,. \tag{3.5b}$$

From (2.3), we get that V and U can be expanded in powers of εA. Therefore, this suggests that we expand

$$\Phi = \Phi_0 + \varepsilon A\Phi_1 + \cdots\,, \qquad N = N_0 + \varepsilon A N_1 + \cdots\,, \qquad \lambda = \varepsilon A\lambda_0 + \cdots\,. \tag{3.6}$$

We first assume that $m = O(1)$ as $\varepsilon \to 0$. Substituting (2.3) and (3.6) into (3.5), and collecting powers of εA, we obtain the following problems on $-\infty < y < \infty$:

$$\Phi_0'' - \Phi_0 + V_0^2N_0 + 2V_0U_0\Phi_0 = 0\,, \tag{3.7a}$$

$$N_0'' - V_0^2N_0 - 2V_0U_0\Phi_0 = 0\,, \tag{3.7b}$$

and

$$\Phi_1'' - \Phi_1 + V_0^2N_1 + 2V_0U_0\Phi_1 = -2V_0V_1N_0 - 2(V_0U_1 + U_0V_1)\Phi_0 + \lambda_0\Phi_0\,, \tag{3.8a}$$

$$N_1'' - V_0^2N_1 - 2V_0U_0\Phi_1 = 2(V_0U_1 + U_0V_1)\Phi_0 + 2V_0V_1N_0\,. \tag{3.8b}$$

The odd solution to the leading-order system (3.7) is

$$\Phi_0 = V_0'\,, \qquad N_0 = U_0'\,. \tag{3.9}$$

We then rewrite (3.8) in matrix form as

$$L\Psi = \begin{pmatrix} \lambda_0 & 0 \\ 0 & 0 \end{pmatrix}\begin{pmatrix} V_{0y} \\ U_{0y} \end{pmatrix} + \begin{pmatrix} -2(V_0U_1 + U_0V_1) & -2V_0V_1 \\ 2(V_0U_1 + U_0V_1) & 2V_0V_1 \end{pmatrix}\begin{pmatrix} V_{0y} \\ U_{0y} \end{pmatrix}\,,$$

where

$$\Psi = \begin{pmatrix} \Phi_1 \\ N_1 \end{pmatrix} \quad \text{and} \quad L\Psi = \Psi'' + \begin{pmatrix} -1 + 2V_0U_0 & V_0^2 \\ -2V_0U_0 & -V_0^2 \end{pmatrix}\Psi. \tag{3.10}$$

The corresponding homogeneous adjoint problem is

$$L^\dagger \Psi^\dagger = \Psi^{\dagger\prime\prime} + \begin{pmatrix} -1+2V_0U_0 & -2V_0U_0 \\ V_0^2 & -V_0^2 \end{pmatrix} \Psi^\dagger = 0\,. \tag{3.11}$$

We look for solutions $\Psi_1^\dagger$ and $\Psi_2^\dagger$ that are odd, with $\Psi_1^\dagger \to 0$ and $\Psi_2^\dagger$ bounded as $|y| \to \infty$.

Multiplying $L\Psi$ by $\Psi^\dagger$, and integrating, we obtain the following solvability condition for the problem for Ψ:

$$\int_{-\infty}^{\infty} \Psi^{\dagger t} L\Psi\, dy = \lambda_0 \int_{-\infty}^{\infty} \Psi_1^\dagger V_0'\, dy + \int_{-\infty}^{\infty} \Psi^{\dagger t} \begin{pmatrix} -2(V_0U_1+U_0V_1) & -2V_0V_1 \\ 2(V_0U_1+U_0V_1) & 2V_0V_1 \end{pmatrix} \begin{pmatrix} V_0' \\ U_0' \end{pmatrix} dy\,. \tag{3.12}$$

Here t denotes transpose. Upon integrating the expression on the left-hand side of this equation by parts, and using $L^\dagger\Psi^\dagger = 0$, we calculate that

$$\int_{-\infty}^{\infty} \Psi^{\dagger t} L\Psi\, dy = \Psi_2^\dagger(\infty) N_1'(\infty) - \Psi_2^\dagger(-\infty) N_1'(-\infty) = \Psi_2^\dagger(\infty) \left[N_1'(\infty) + N_1'(-\infty)\right]\,. \tag{3.13}$$

Substituting (3.13) into (3.12), we get

$$2I_2\lambda_0 = \Psi_2^\dagger(\infty) \left[N_1'(+\infty) + N_1'(-\infty))\right] - I_1\,, \tag{3.14a}$$

where I_1 and I_2 are defined by

$$I_2 = \int_0^\infty \Psi_1^\dagger V_0'\, dy\,, \qquad I_1 = \int_{-\infty}^{\infty} \Psi^{\dagger t} \begin{pmatrix} -2\,(V_0U_0)' & -\left(V_0^2\right)' \\ 2\,(V_0U_0)' & \left(V_0^2\right)' \end{pmatrix} \begin{pmatrix} V_1 \\ U_1 \end{pmatrix} dy\,. \tag{3.14b}$$

The integral defining I_1 can be evaluated explicitly by using the equation satisfied by $W = \begin{pmatrix} V_1' \\ U_1' \end{pmatrix}$. By differentiating (2.5) with respect to y, we obtain that W satisfies

$$LW = \begin{pmatrix} -2\,(V_0U_0)' & -\left(V_0^2\right)' \\ 2\,(V_0U_0)' & \left(V_0^2\right)' \end{pmatrix} \begin{pmatrix} V_1 \\ U_1 \end{pmatrix}\,.$$

Therefore, using integration by parts, I_1 in (3.14b) can be calculated as

$$I_1 = \int_{-\infty}^{\infty} \Psi^{\dagger t} LW\, dy = \Psi_2^\dagger(+\infty) U_1''(+\infty) - \Psi_2^\dagger(-\infty) U_1''(-\infty) = -2\Psi_2^\dagger(+\infty)\,. \tag{3.15}$$

Here we have used $U_1''(\pm\infty) = -1$ from (2.14) and the result that Ψ_2 is odd. Substituting (3.15) into (3.14a), we get that

$$\lambda_0 = -\alpha \left(\frac{N_1'(+\infty) + N_1'(-\infty)}{2} + 1 \right)\,, \qquad \alpha \equiv \frac{-\Psi_2^\dagger(+\infty)}{\int_0^\infty \Psi_1^\dagger V_0'\, dy}\,. \tag{3.16}$$

To determine $N_1'(\pm\infty)$, we must determine an appropriate outer solution for the eigenpair of (3.3). In the outer region, we obtain from (3.3b) that η satisfies

$$\eta_{x_1 x_1} - \left(1 + m^2 + \tau\lambda\right)\eta = 2u_e v_e \phi + v_e^2 \eta\,, \tag{3.17}$$

with $\eta_{x_1}(\pm l) = 0$. The right-hand side of (3.17) is localized near $x_1 = 0$. Therefore, using (3.4) we calculate for $x_1 = O(\varepsilon)$ that

$$2u_e v_e \phi + v_e^2 \eta \sim \frac{2}{\varepsilon A}\left(UV\Phi\right) + \frac{1}{\varepsilon A}\left(V^2 N\right)\,. \tag{3.18}$$

By expanding V, U, Φ, and N, in powers of εA as in (2.3) and (3.6), we get that (3.18) becomes

$$2u_e v_e \phi + v_e^2 \eta \sim \frac{1}{\varepsilon A}\left(U_0 V_0^2\right)' + N_1''\,. \tag{3.19}$$

Therefore, since $2B = \int_{-\infty}^{\infty} U_0 V_0^2\,dy$ and $B = A\tanh l$, we obtain in the sense of distributions that η satisfies

$$\eta_{x_1 x_1} - \left(1 + m^2 + \tau\lambda\right)\eta = 2\varepsilon\tanh(l)\delta'(x_1) + \varepsilon\left[N_1'(+\infty) - N_1'(-\infty)\right]\delta(x_1)\,, \tag{3.20}$$

with $\eta_{x_1}(\pm l) = 0$. The matching condition of the inner and outer solutions for η requires that

$$\frac{\varepsilon}{A}\left(N_0 + \varepsilon A N_1 + \cdots\right) \sim \eta\left(0^{\pm}\right) + \varepsilon y \eta_{x_1}\left(0^{\pm}\right) + \cdots\,. \tag{3.21}$$

Since $N_0 = U_0'$ satisfies $N_0(\pm\infty) = \pm B$, we get from this matching condition that

$$\eta\left(0^{\pm}\right) = \pm\frac{\varepsilon B}{A} = \pm\varepsilon\tanh(l)\,, \qquad N_1'(\pm\infty) = \varepsilon^{-1}\eta_{x_1}\left(0^{\pm}\right)\,. \tag{3.22}$$

Solving (3.20) for $\eta(x_1)$, we obtain that

$$\eta(x_1) = \begin{cases} \varepsilon\tanh l\,\frac{\cosh\theta(l-x_1)}{\cosh(\theta l)}\,, & 0 < x_1 < l\,, \\ -\varepsilon\tanh l\,\frac{\cosh\theta(l+x_1)}{\cosh(\theta l)}\,, & -l < x_1 < 0\,, \end{cases}$$

where θ is defined by $\theta \equiv \sqrt{1 + \tau\lambda + m^2}$. From (3.22) this yields that

$$N_1'(+\infty) = -\theta\tanh(\theta l)\tanh l\,, \qquad N_1'(-\infty) = -\theta\tanh(\theta l)\tanh l\,. \tag{3.23}$$

Finally, substituting (3.23) into (3.16), and using (3.6), we obtain an equation for λ. We summarize our result as follows:

Proposition 3 *Consider a stripe equilibrium solution (U_0, V_0) of (1.2) in the high feed-rate and intermediate regimes, as given by Propositions 1 and 2, respectively. Suppose that $m = O(1)$ as $\varepsilon \to 0$. Then, any instability of the linearized problem has the form*

$$U \sim U_0 \left(y + c e^{imx_2} e^{\lambda t} \right) , \qquad V \sim V_0 \left(y + c e^{imx_2} e^{\lambda t} \right) ,$$

where $y = \varepsilon^{-1} x_1$, c is a small constant, and λ satisfies the transcendental equation

$$\lambda \sim -\varepsilon A \alpha \left(1 - \theta \tanh(\theta l) \tanh l\right) . \tag{3.24}$$

Here θ and α are defined by

$$\theta \equiv \sqrt{1 + \lambda\tau + m^2} , \qquad \alpha \equiv \frac{-\Psi_2^\dagger(+\infty)}{\int_0^\infty \Psi_1^\dagger V_0' \, dy} . \tag{3.25}$$

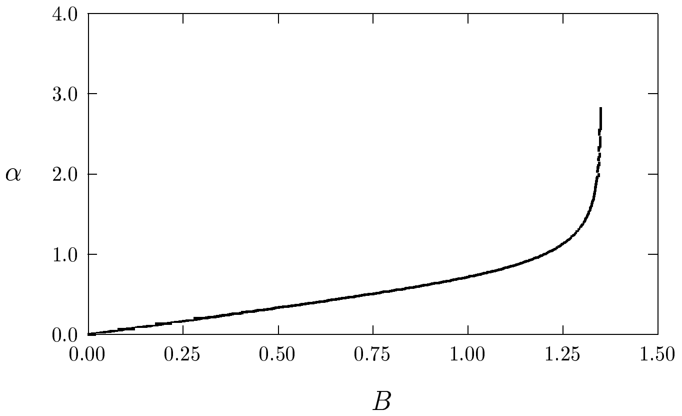

Figure 2: Plot of α, defined in (3.25), versus B along the primary solution branch of the γ versus B bifurcation diagram. The right endpoint of this curve corresponds to the fold point $B = 1.347$.

The constant α depends on the core solution through the parameter B, where B is defined in Proposition 1. In the high feed-rate regime where $B = O(1)$, α can only be determined numerically as was done in [13]. From Fig. 2, where we plot α versus B along the primary branch, we conclude that $\alpha > 0$ at each point along the primary branch. As a partial analytical confirmation of the sign of α, we can use Proposition 2 to calculate α in the intermediate regime where $B = 3\delta \ll 1$. From Proposition 2, the homogeneous adjoint problem (3.11) in the intermediate regime reduces to

$$\psi_{1yy}^\dagger + (-1 + 2w)\psi_1^\dagger \sim 2w\psi_2^\dagger , \qquad \psi_{2yy}^\dagger + \delta^2 w^2 \left(\psi_1^\dagger - \psi_2^\dagger \right) \sim 0 . \tag{3.26}$$

Therefore, we get $\psi_1^\dagger = w_y + O(\delta^2)$ and $\psi_2^\dagger = -\frac{\delta^2}{3}\int_0^y [w(s)]^3\, ds + O(\delta^4)$. Since $V_0 \sim \delta w$ and $w(y) = \frac{3}{2}\mathrm{sech}^2(y/2)$ from Proposition 2, we obtain that

$$\alpha \equiv -\frac{\Psi_2^\dagger(\infty)}{\int_0^\infty \Psi_1^\dagger V_{0y}\, dy} \sim \frac{\delta}{3}\left(\frac{\int_0^\infty w^3\, dy}{\int_0^\infty w_y^2\, dy}\right) \sim 2\delta\,. \tag{3.27}$$

In summary, in the intermediate regime $B \sim 3\delta$, where $O(\varepsilon^{1/2}) \ll \delta \ll O(1)$, we get that $\alpha \sim 2\delta$. This limiting expression can be rewritten by using $\delta \sim A/[3\coth(l)]$ and $B = A\tanh(l)$ to obtain

$$\alpha \sim \frac{2A}{3}\tanh(l) \sim \frac{2B}{3} > 0\,, \qquad \text{for} \quad A \ll 1\,. \tag{3.28}$$

We will assume that $\tau = O(1)$ as $\varepsilon \to 0$, so that with $\lambda = O(\varepsilon)$ we get that $\theta \sim \sqrt{1+m^2}$. Therefore, when $\tau = O(1)$, (3.24) reduces to

$$\lambda \sim -A\varepsilon\alpha\left(1 - \sqrt{m^2+1}\tanh l \tanh(l\sqrt{m^2+1})\right)\,. \tag{3.29}$$

From (3.29), we observe that λ is negative for small m, but is positive when m is large enough. We summarize the result as follows:

Corollary 4 *Consider a stripe equilibrium solution (U_0, V_0) of (1.2) in the high feed-rate and intermediate regimes, as given by Propositions 1 and 2, respectively. Suppose that $m = O(1)$ and $\tau = O(1)$ as $\varepsilon \to 0$. Then, the stripe solution is unstable for modes m with $m > m_b$, where m_b is the unique root of the transcendental equation*

$$\sqrt{1+m^2}\tanh l \tanh\left(l\sqrt{1+m^2}\right) = 1\,. \tag{3.30}$$

In Fig. 3 we plot the domain half-length l versus the first unstable mode m_b. It is clear that the first unstable mode m_b satisfies $m_b \sim 0$ as $l \to \infty$. Additionally, it easy to see that $m_b \sim \frac{z}{l}$ as $l \to 0$, where $z = 1.1997$ is the unique root of $z\tanh z = 1$.

Next, we consider the range of m where $O(1) \ll m \ll O(\varepsilon^{-1})$. In the inner region, we expand the solution to the eigenvalue problem (3.5) in the form

$$\Phi = V_0^{'} + \varepsilon m\Phi_1 + \cdots\,, \quad \Phi = U_0^{'} + \varepsilon m N_1 + \cdots\,, \quad \lambda = \varepsilon m\lambda_0 + \cdots\,. \tag{3.31}$$

We assume that $\varepsilon m \gg \varepsilon A$ so that the correction to the eigenfunction is asymptotically larger than the correction to the leading order core solution given in (2.3). When $A = O(1)$, this condition implies

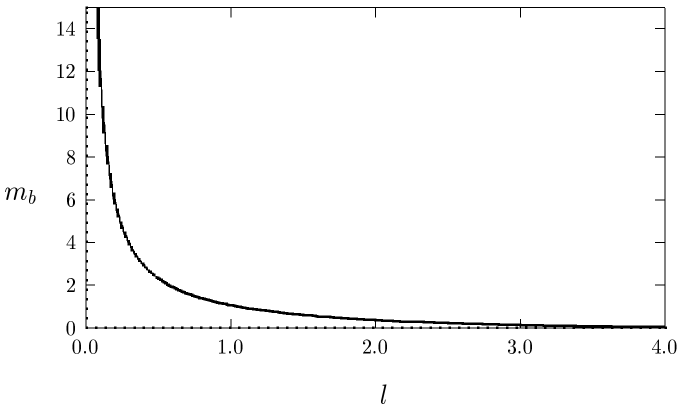

Figure 3: Plot of the smallest unstable mode m_b versus the domain half-length l. Above this curve we have instability.

that $m \gg O(1)$. Substituting (3.31) and (2.3) into (3.5), we collect terms proportional to εm to get the following problem for Φ_1 and N_1 on $-\infty < y < \infty$:

$$\Phi_1'' - \Phi_1 + V_0^2 N_1 + 2V_0 U_0 \Phi_1 = \lambda_0 V_0^{'}\,, \tag{3.32a}$$

$$N_1'' - V_0^2 N_1 - 2V_0 U_0 \Phi_1 = 0\,. \tag{3.32b}$$

To determine λ_0, we multiply (3.32) by the adjoint solution $\Psi^\dagger$, which satisfies (3.11). By integrating over the domain, we obtain that

$$\int_{-\infty}^{\infty} \Psi^{\dagger t} L \Psi \, dy = \Psi_2^\dagger(\infty) \left[N_1^{'}(\infty) + N_1^{'}(-\infty) \right] = \lambda_0 \int_{-\infty}^{\infty} \Psi_1^\dagger V_0' \, dy\,. \tag{3.33}$$

To determine $N_1^{'}(\pm\infty)$, we proceed as in the analysis of (3.17)–(3.19). Since $m \gg O(1)$, we obtain, on either side of the stripe location $x_1 = 0$, that the outer solution for η asymptotically satisfies

$$\eta_{x_1 x_1} - m^2 \eta = 0\,, \quad -l < x_1 < l\,; \qquad \eta_{x_1}(\pm l) = 0\,. \tag{3.34}$$

The matching condition for the inner and outer solutions for η is that

$$\frac{\varepsilon}{A} \left(U_0^{'}(\pm\infty) + \varepsilon m N_1 + \cdots \right) \sim \eta\left(0^\pm\right) + \varepsilon y \eta_{x_1}\left(0^\pm\right) + \cdots\,. \tag{3.35}$$

Since $U_0^{'}(\pm\infty) = \pm B$, this yields that $\eta(0^\pm) = \pm\varepsilon B/A = \pm\varepsilon \tanh l$, and

$$N_1^{'}(\pm\infty) = \frac{A}{\varepsilon m} \eta_{x_1}(0^\pm)\,. \tag{3.36}$$

The solution to (3.34) is therefore

$$\eta(x_1) \sim (\varepsilon \tanh l) e^{-m x_1}\,, \quad x_1 > 0\,; \qquad \eta(x_1) \sim -(\varepsilon \tanh l) e^{m x_1}\,, \quad x_1 < 0\,. \tag{3.37}$$

From (3.36) we get that $N_1'(\pm\infty) = -A \tanh l$. Then, we substitute this result into (3.33) to calculate λ_0. Since $\lambda = \varepsilon m \lambda_0 + \cdots$, we conclude that

$$\lambda \sim \varepsilon m \alpha A \tanh l\,, \qquad \alpha \equiv -\frac{\Psi_2^\dagger(\infty)}{\int_0^\infty \Psi_1^\dagger V_{0y}\, dy}\,, \tag{3.38}$$

which is valid when $O(1) \ll m \ll O(\varepsilon^{-1})$ and $A = O(1)$. Since $\alpha > 0$ along the primary branch of the γ versus B curve, we conclude from (3.38) that, when $A = O(1)$, all of the modes with $O(1) \ll m \ll O(\varepsilon^{-1})$ are unstable along this branch due to a real positive eigenvalue. As a remark, (3.38) can also be obtained formally by letting $m \to \infty$ in (3.24) of Proposition 3.

To determine the re-stabilization threshold for the zigzag instability of a stripe in the high feed-rate regime where $A = O(1)$, we must consider the regime where $m = O(\varepsilon^{-1})$. In this regime, we introduce m_0 by $m = m_0 \varepsilon^{-1}$, where $m_0 = O(1)$. From (3.5), the corresponding leading-order eigenvalue problem, defined on $-\infty < y < \infty$, is

$$(\lambda + m_0^2)\Phi_0 = \Phi_0'' - \Phi_0 + V_0^2 N_0 + 2V_0 U_0 \Phi_0\,, \tag{3.39a}$$

$$m_0^2 N_0 = N_0'' - V_0^2 N_0 - 2V_0 U_0 \Phi_0\,. \tag{3.39b}$$

We seek an odd eigenfunction to this problem for which $\Phi_0 \to 0$ and $N_0 \to 0$ as $y \to \pm\infty$.

In the high feed-rate regime, the system (3.39) can only be solved numerically. To do so, we discretize (3.39) on a long interval $[0, L]$ using centered finite differences, ensuring that Φ_0 and N_0 are odd functions so that $N_0(0) = \Phi_0(0) = 0$. Choosing a meshsize $h = L/n$, where $n > 1$, we label $y_1 = h$ and $y_n = L$. This leads to the discrete eigenvalue problem

$$\left(\mathcal{M} - \left(1 + m_0^2\right) I + \Lambda_2\right) \boldsymbol{\Phi_0} + \Lambda_1 \boldsymbol{N_0} = \lambda \boldsymbol{\Phi_0}\,, \qquad \left(\mathcal{M} - m_0^2 I - \Lambda_1\right) \boldsymbol{N_0} = \Lambda_2 \boldsymbol{\Phi_0}\,, \tag{3.40a}$$

so that

$$\left(\mathcal{M} - \left(1 + m_0^2\right) I + \Lambda_2 + \Lambda_1 \left(\mathcal{M} - m_0^2 I - \Lambda_1\right)^{-1} \Lambda_2\right) \boldsymbol{\Phi_0} = \lambda \boldsymbol{\Phi_0}\,. \tag{3.40b}$$

Here $\boldsymbol{\Phi_0} = (\Phi_0(y_1), \ldots, \Phi_0(y_n))^t$, $\boldsymbol{N_0} = (N_0(y_1), \ldots, N_0(y_n))^t$, and the matrices Γ_1, Γ_2, and $\mathcal{M}$, are defined by

$$\Lambda_1 \equiv \begin{pmatrix} V_0^2(y_1) & 0 & \cdots & 0 \\ 0 & \ddots & \cdots & 0 \\ \vdots & \vdots & \ddots & \vdots \\ 0 & 0 & \cdots & V_0^2(y_n) \end{pmatrix}, \qquad \Lambda_2 \equiv \begin{pmatrix} 2U_0(y_1)V_0(y_1) & 0 & \cdots & 0 \\ 0 & \ddots & \cdots & 0 \\ \vdots & \vdots & \ddots & \vdots \\ 0 & 0 & \cdots & 2U_0(y_n)V_0(y_n) \end{pmatrix}, \tag{3.40c}$$

and

$$\mathcal{M} \equiv \frac{1}{h^2} \begin{pmatrix} -2 & 1 & 0 & \cdots & 0 & 0 & 0 \\ 1 & -2 & 1 & \ddots & \ddots & 0 & 0 \\ 0 & \ddots & \ddots & \ddots & \ddots & \ddots & 0 \\ \vdots & \ddots & \ddots & \ddots & \ddots & \ddots & \vdots \\ 0 & \ddots & \ddots & \ddots & \ddots & \ddots & 0 \\ 0 & 0 & \ddots & \ddots & 1 & -2 & 1 \\ 0 & 0 & 0 & \cdots & 0 & 2 & -2 \end{pmatrix} . \tag{3.40d}$$

Our computational results show that there is a critical value m_{0u} of m_0 for which $\text{Re}(\lambda) < 0$ for $m_0 > m_{0u}$ and $\text{Re}(\lambda) > 0$ for $m_0 < m_{0u}$. This re-stabilization value m_{0u} is computed numerically from the discrete eigenvalue problem using LAPACK [1] on a domain with $L = 12$ and $n = 200$ meshpoints. Increasing the number of meshpoints and the domain length did not change the results significantly. In Fig. 4 we plot the critical mode m_{0u}, corresponding to $\lambda = 0$, for each point along the primary branch of the γ versus B bifurcation diagram. Notice that the critical mode m_{0u} tends to zero as $\gamma \to 1.5$ (and consequently $B \to 0$). Therefore, this suggests that as we approach the intermediate regime the re-stablization value of m is no longer $O(\varepsilon^{-1})$.

We summarize our stability results obtained so far in the following statement:

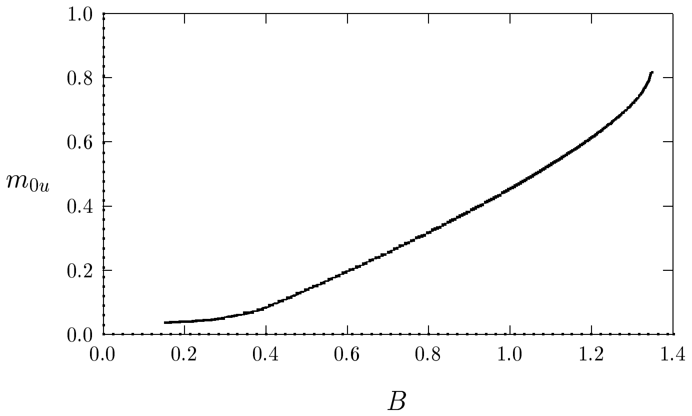

Figure 4: Plot of the re-stablization value m_{0u} (with $m_u = \varepsilon^{-1} m_{0u}$) versus B computed from (3.39) at each point along the primary branch of the γ versus B bifurcation diagram. Above this curve we have stability with respect to zigzag perturbations.

Proposition 5 *Consider a stripe equilibrium solution (U_0, V_0) of (1.2) as given by Proposition 1. Suppose that $\varepsilon \ll 1$ and $\tau = O(1)$. Then, all zigzag-type perturbations of the form*

$$U \sim U_0(y) + ce^{imx_2}e^{\lambda t}\phi\,, \qquad V \sim V_0(y) + ce^{imx_2}e^{\lambda t}\eta\,,$$

are unstable in the zone $m_b < m < \varepsilon^{-1}m_{0u}$, and are stable outside of this zone. Here m_b is the root of (3.30), which depends on the domain half-length l. The threshold m_{0u}, plotted in Fig. 4, is independent of l but depends on the value of B along the primary branch of the γ versus B bifurcation diagram.

Fig. 4 suggests that the re-stabilization threshold satisfies $m_{0u} \to 0$ as $B \to 0$. This suggests that all of the modes with $m = O(\varepsilon^{-1})$ should be stable in the intermediate regime where $O(\varepsilon^{1/2}) \ll A \ll O(1)$. We now show this analytically by using the limiting form of V_0 and U_0 in the intermediate regime as given in Proposition 2. From (2.21) we calculate

$$V_0^2 = \delta^2 w^2 + 2\delta^4 w v_1 + \cdots\,, \qquad U_0 V_0 = w + \delta^2\left(v_1 + u_1 w\right) + \cdots\,. \tag{3.41}$$

Upon substituting (3.41) into (3.39), it follows that we should expand

$$\Phi_0 = \Phi_{00} + \delta^2\Phi_{01} + \cdots\,; \qquad N_0 = N_{00} + \delta^2 N_{01} + \cdots\,; \qquad m_0 = \delta\mu + \cdots\,; \qquad \lambda = \lambda_0\delta^2 + \cdots\,. \tag{3.42}$$

Substituting (3.41) and (3.42) into (3.39), we get the leading-order problem on $-\infty < y < \infty$:

$$L_0\Phi_{00} \equiv \Phi_{00}^{''} - \Phi_{00} + 2w\Phi_{00} = 0\,; \qquad N_{00}^{''} = 2w\Phi_{00}\,. \tag{3.43}$$

From collecting terms of $O(\delta^2)$ we obtain an equation for Φ_{01}

$$L_0\Phi_{01} = \left(\lambda_0 + \mu^2\right)\Phi_{00} - w^2 N_{00} - 2(v_1 + u_1 w)\Phi_{00}\,. \tag{3.44}$$

Comparing (3.43) with (2.22) and (2.23), we conclude that $\Phi_{00} = w^{'}$ and $N_{00} = u_1^{'}$, where $w(y) = \frac{3}{2}\text{sech}^2(y/2)$ and u_1 satisfies (2.23). Since $L_0 w^{'} = 0$, the solvability condition for (3.44) yields that

$$\left(\lambda_0 + \mu^2\right)\int_{-\infty}^{\infty} w^{'2}\,dy = \int_{-\infty}^{\infty} w^2 w^{'} u_1^{'}\,dy + 2\int_{-\infty}^{\infty}\left(u_1 w + v_1\right) w^{'2}\,dy\,. \tag{3.45}$$

To simplify (3.45) we differentiate the equation (2.24) for v_1 to get

$$L_0 v_1^{'} = -w^2 u_1^{'} - 2(v_1 + u_1 w)w^{'}\,. \tag{3.46}$$

Since $L_0 w^{'} = 0$, the solvability condition for (3.46) readily yields that the right hand-side of (3.45) is identically zero. Therefore, (3.45) reduces to $\lambda_0 = -\mu^2$. From (3.42) we get $\lambda \sim -\delta^2\mu^2$ and $m = \delta\mu/\varepsilon$, which implies that

$$\lambda \sim -(\varepsilon m)^2\,. \tag{3.47}$$

This shows that all of the modes with $m = O(\delta/\varepsilon)$ are stable in the intermediate regime.

To determine the re-stabilization threshold in the intermediate regime, we must return to (3.32). Recall from the discussion above that (3.32) is not uniformly valid in the intermediate since we have neglected the term $\varepsilon^2 m^2 \Phi$ in (3.5). This is seen by comparing the terms εA with $\varepsilon^2 m^2$ in this regime. In this regime, we get from Proposition 2 that $A = O(\delta)$ with $O(\varepsilon^{1/2}) \ll \delta \ll 1$. Therefore, when $m = O\left(\delta^2/\varepsilon\right)$, we conclude that $\varepsilon^2 m^2 \gg \varepsilon A$ when $\delta \gg O(\varepsilon^{1/3})$, and $\varepsilon^2 m^2 \ll \varepsilon A$ when $O(\varepsilon^{1/2}) \ll \delta \ll O(\varepsilon^{1/3})$. Therefore, we must include the term $\varepsilon^2 m^2 \Phi$ in the analysis. Formally re-writing (3.32a), but now including the term $\varepsilon^2 m^2 \Phi_0$, we obtain

$$\Phi_1'' - m\varepsilon V_0' - \Phi_1 + V_0^2 N_1 + 2V_0 U_0 \Phi_1 = \lambda_0 V_0' \,, \tag{3.48}$$

This shows that we need only replace λ_0 with $\lambda_0 + m\varepsilon$. Then, proceeding as in the derivation of (3.38), we obtain that

$$\lambda_0 + \varepsilon m \sim \alpha A \tanh l \,. \tag{3.49}$$

From Proposition 2 and (3.28) we recall that $B = A \tanh l \sim 3\delta$ and $\alpha \sim 2\delta$ in the intermediate regime. Therefore, with $\lambda = \varepsilon m \lambda_0$, (3.49) becomes

$$\lambda \sim \varepsilon m \left(6\delta^2 - \varepsilon m\right) \,. \tag{3.50}$$

This expression shows that the re-stabilization threshold occurs at the asymptotic value $m \sim 6\delta^2/\varepsilon$. Therefore, in the intermediate regime, the threshold m_{0u} in Proposition 5 is simply

$$m_{0u} \sim 6\delta^2 \,. \tag{3.51}$$

Notice that when $m = O(\varepsilon^{-1})$, (3.50) reduces asymptotically to (3.47).

As a remark, in all of the analysis in this section we have assumed that $\tau = O(1)$ as $\varepsilon \to 0$. If we were to allow $\tau = O(\varepsilon^{-1})$, then for each fixed value of m we could get a zigzag instability due a Hopf bifurcation when τ is increased past some threshold. This type of Hopf bifurcation was studied in [13] for a one-dimensional spike solution corresponding to $m = 0$. We will not consider the case of asymptotically large τ here.

4 Breakup Instabilities of a Stripe

In this section we study the stability with respect to the large eigenvalues of the stripe equilibrium solution constructed in §2. These instabilities are found to be the mechanism through which a stripe equilibrium breaks up into a sequence of spots.

As in the study in §3 of the small eigenvalues, we look for a normal mode solution in the inner region $x_1 = O(\varepsilon)$ in the form

$$v = \frac{1}{\varepsilon}\left(V(y) + e^{\lambda t} e^{imx_2}\Phi(y)\right) , \qquad u = \frac{\varepsilon}{A}\left(U(y) + e^{\lambda t} e^{imx_2} N(y)\right) , \tag{4.1}$$

where $y = \varepsilon^{-1}x_1$ and U, V, Φ, and N, have power series expansions in powers of εA. In contrast to the study of the small eigenvalues of §3, we now look for even functions Φ and N. Substituting (4.1) into (1.2), and assuming that $\tau = O(1)$, we obtain the following leading-order eigenvalue problem on $-\infty < y < \infty$:

$$\lambda\Phi_0 = \Phi_0'' - (1+\mu)\,\Phi_0 + V_0^2 N_0 + 2V_0U_0\Phi_0 \,, \tag{4.2a}$$

$$0 = N_0'' - \mu N_0 - V_0^2 N_0 - 2V_0U_0\Phi_0 \,. \tag{4.2b}$$

Here we have defined μ by $\mu \equiv \varepsilon^2 m^2$.

To determine the instability band for (4.2), we discretize (4.2) on a long interval $[0, L]$ using centered finite differences, ensuring that Φ_0 and N_0 are even functions and that $N_{0y} = 0$ at $y = L$. The resulting matrix eigenvalue problem is similar to that in (3.40), except for slight differences in the matrix structure due to the different parity of the breakup eigenfunction. Our computational results show that there are values μ_1 and μ_2 for which $\text{Re}(\lambda) > 0$ for $\mu_1 < \mu < \mu_2$, and $\text{Re}(\lambda) < 0$ for $0 < \mu < \mu_1$ and $\mu > \mu_2$. This instability band is determined from numerical computations of the discrete eigenvalue problem using LAPACK [1] on a domain with $L = 12$ and $n = 200$ meshpoints. Increasing the number of meshpoints and the domain length did not change the results significantly. In Fig. 5 and in Table 1, we give numerical results for μ_1 and μ_2 versus B along the primary branch of the γ versus B curve.

Although we are not able to calculate μ_1 and μ_2 analytically in the high feed-rate regime, we can asymptotically calculate these critical values, at which $\lambda = 0$, in the intermediate regime where $B = 3\delta \ll 1$ with $O(\varepsilon^{1/2}) \ll \delta \ll O(1)$.

In the intermediate regime we use Proposition 2 for V_0 and U_0. In this way, (4.2) reduces to

$$(\mu+\lambda)\Phi_0 \sim \Phi_0'' - \Phi_0 + 2\left(w + O(\delta^2)\right)\Phi_0 + \left(\delta^2 w^2 + O(\delta^4)\right) N_0 \,, \tag{4.3a}$$

$$\mu N_0 \sim N_0'' - 2\left(w + O(\delta^2)\right)\Phi_0 - \left(\delta^2 w^2 + O(\delta^4)\right) N_0 \,. \tag{4.3b}$$

The balance of the various terms in the first equation gives rise to two possibilities: either $O(N_0)\delta^2 \ll O(\Phi_0)$ or $O(N_0)\delta^2 = O(\Phi_0)$. In the former case, the leading order equation for Φ_0 on $-\infty < y < \infty$ is

$$(\mu+\lambda)\Phi_0 = \Phi_0'' - \Phi_0 + 2w\Phi_0 \,, \tag{4.4}$$

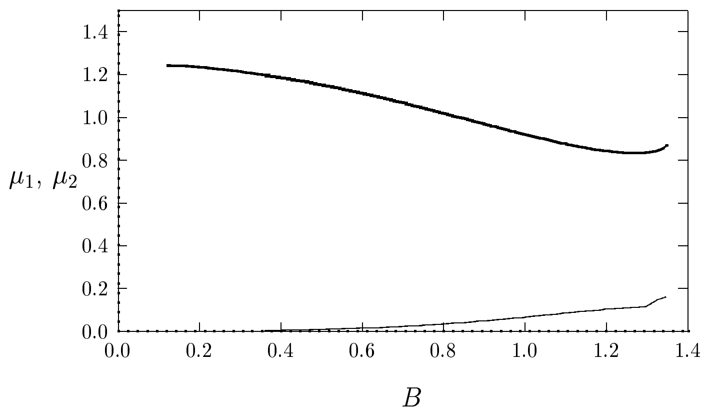

Figure 5: Plot of μ_1 (heavy solid curve) and μ_2 (solid curve) versus B computed from (4.2) at each point along the primary branch of the γ versus B bifurcation diagram. In terms of m, the thresholds are $m_j = \sqrt{\mu_j}/\varepsilon$ for $j = 1, 2$.

with $\Phi_0 \to 0$ as $|y| \to \infty$. This is a well-known eigenvalue problem (see for instance [18]). It has a unique positive eigenvalue $\mu + \lambda = \frac{5}{4}$. This gives the upper bound of $\mu_2 = \frac{5}{4}$ for the instability band.

For the second possibility, we must expand

$$N_0 = \frac{1}{\delta^2}\left(N_{00} + \delta^2 N_{01} + \cdots\right), \qquad \mu = \delta^2 \mu_0 + \cdots, \qquad \Phi_0 = \Phi_{00} + \delta^2 \Phi_{01} + \cdots. \tag{4.5}$$

Substituting this expansion into (4.3), we get that N_{00} satisfies $N_{00}'' = 0$. Therefore, N_{00} is a constant to be determined. The leading-order equation for Φ_0 is

$$\lambda \Phi_{00} = \Phi_{00}'' - \Phi_{00} + 2w\Phi_{00} + N_{00} w^2, \tag{4.6}$$

with $\Phi_{00} \to 0$ as $|y| \to \infty$. To determine N_{00}, we must match the inner solution to the outer solution.

In the outer region, we obtain from (3.3b) that η satisfies

$$\eta_{x_1 x_1} - \left(1 + m^2 + \tau\lambda\right)\eta = 2u_e v_e \phi + v_e^2 \eta, \tag{4.7}$$

with $\eta_{x_1}(\pm l) = 0$. The right-hand side of (4.7) is localized near $x_1 = 0$. Using Proposition 2 for solutions in the intermediate regime we obtain that

$$2u_e v_e \phi + v_e^2 \eta \sim \frac{2w}{\varepsilon A}\Phi_{00} + \frac{w^2}{\varepsilon A} N_{00}. \tag{4.8}$$

γ	B	μ_1	μ_2
1.464	0.40	0.003713	1.188
1.443	0.50	0.007010	1.154
1.419	0.60	0.01249	1.113
1.390	0.70	0.02093	1.069
1.357	0.80	0.03277	1.020
1.319	0.90	0.04796	0.9700
1.277	1.00	0.06588	0.9208
1.220	1.12	0.08830	0.8695
1.140	1.25	0.1096	0.8345
1.100	1.30	0.1156	0.8358
1.020	1.347	0.1617	0.8724

Table 1: The values of μ_2 and μ_1 as defined in Proposition 7 along the primary branch of the γ versus B bifurcation diagram.

Therefore, we obtain the following problem for $\eta(x_1)$:

$$\eta_{x_1x_1} - \left(1 + m^2 + \tau\lambda\right)\eta = \left(\frac{2}{A}\int_{-\infty}^{\infty} w\Phi_{00}\,dy + \frac{N_{00}}{A}\int_{-\infty}^{\infty} w^2\,dy\right)\delta(x_1)\,, \qquad -l < x_1 < l\,, \tag{4.9}$$

with $\eta_{x_1}(\pm l) = 0$. The solution for η is

$$\eta(x_1) = -\left(\frac{2}{A}\int_{-\infty}^{\infty} w\Phi_{00}\,dy + \frac{N_{00}}{A}\int_{-\infty}^{\infty} w^2\,dy\right)G_m(x_1)\,, \tag{4.10}$$

where $G_m(x_1)$ is the Green's function satisfying

$$G_{mx_1x_1} - \theta^2 G_m = -\delta(x_1)\,, \quad -l < x_1 < l\,; \qquad G_{mx_1}(\pm l) = 0\,. \tag{4.11}$$

Here $\theta \equiv \sqrt{1 + m^2 + \tau\lambda}$. The matching condition for the inner and outer solutions is that

$$\frac{\varepsilon}{A}\left(\delta^{-2}N_{00} + \cdots\right) \sim \eta(0) + \cdots\,. \tag{4.12}$$

This yields that $\eta(0) = \varepsilon\delta^{-2}N_{00}/A$. By calculating the solution to (4.11), and evaluating (4.10) at $x_1 = 0$, we obtain an equation for the unknown constant N_{00}

$$N_{00}\left(\frac{G_m(0)}{A}\int_{-\infty}^{\infty} w^2\,dy + \frac{\varepsilon}{A\delta^2}\right) = -\frac{2}{A}\left(\int_{-\infty}^{\infty} w\Phi_{00}\,dy\right)G_m(0)\,. \tag{4.13}$$

Using (4.11), we calculate $G_m(0)$ as

$$G_m(0) = \frac{\coth(l\theta)}{2\theta}, \qquad \theta \equiv \sqrt{1+m^2+\tau\lambda}\,. \tag{4.14}$$

Solving (4.13) for N_{00}, noting that $\int_{-\infty}^{\infty} w^2\,dy = 6$, and substituting the result into (4.6), we obtain the following nonlocal eigenvalue problem for Φ_{00} on $-\infty < y < \infty$:

$$\Phi_{00}'' - \Phi_{00} + 2w\Phi_{00} - \chi w^2 \frac{\int_{-\infty}^{\infty} w\Phi_{00}\,dy}{\int_{-\infty}^{\infty} w^2\,dy} = \lambda\Phi_{00}\,, \tag{4.15}$$

with $\Phi_{00} \to 0$ as $|y| \to \infty$. Here χ is defined by

$$\chi \equiv 2\left[1 + \frac{\varepsilon}{6\delta^2 G_m(0)}\right]^{-1}. \tag{4.16}$$

Next, we use the following fundamental lemma from [29]:

Lemma 6 *(Wei, [29]) Let $\chi \geq 0$, and consider the nonlocal eigenvalue problem*

$$\lambda\Phi = \Phi'' - \Phi + 2w\Phi - \chi w^2 \frac{\int w\Phi\,dy}{\int w^2\,dy}, \qquad -\infty < y < \infty\,,$$

with $\Phi \to 0$ as $|y| \to \infty$. Then, there are eigenvalues with Re$(\lambda) > 0$ if and only if $\chi < 1$.

We now use this lemma to determine the lower limit of the stability band. In the intermediate regime we have that $\delta \gg O(\varepsilon^{1/2})$. Therefore, if $m = O(1)$, we get from (4.16) that $\chi \sim 2$. Therefore, from the Lemma of [29], we conclude that all the modes with $m = O(1)$ are stable. Alternatively, when $m \gg 1$, we calculate from (4.14) that $G_m(0) \sim \frac{1}{2m}$. Therefore, from (4.16), we obtain that

$$\chi \sim 2\left[1 + \frac{m\varepsilon}{3\delta^2}\right]^{-1}.$$

The threshold $\chi = 1$ for instability from the fundamental Lemma of [29] is achieved when

$$m\varepsilon = 3\delta^2\,.$$

This yields the lower limit μ_1 of the instability band in the intermediate regime. We summarize our result for breakup instabilities in the following statement:

Proposition 7 *Let $\varepsilon \to 0$ and $\tau = O(1)$. In the intermediate regime, the stripe equilibrium solution as given by Proposition 2 is unstable with respect to breakup instabilities if and only if the following inequality holds:*

$$3\delta^2 < \varepsilon m < \frac{\sqrt{5}}{2}\,. \tag{4.17}$$

In the high feed-rate regime, the instability band along the primary solution branch of the γ versus B curve is given by

$$\sqrt{\mu_1} < \varepsilon m < \sqrt{\mu_2}\,, \tag{4.18}$$

where $\mu_1 = \mu_1(B)$ and $\mu_2 = \mu_2(B)$ are given in Fig. 5 and in Table 1.

5 Equilibria and Stability of a Ring Solution

In this section we modify the methods of §2–4 to obtain analogous results for the stability of an equilibrium ring solution for the Gray-Scott model (1.2) in the disk domain

$$\Omega = \{x : |x| \equiv \rho < R\}.$$

We begin by constructing an equilibrium ring solution centered at $\rho = \rho_0$, for some ρ_0 with $0 < \rho_0 < R$ to be determined. Although equilibrium ring solutions were constructed in [15] and [19], we include the derivation here as many of the formulae are needed for the stability analysis.

In the inner region near ρ_0, we proceed as in §2 by looking for a solution of the form

$$v = \frac{V}{\varepsilon}\,, \qquad u = \frac{\varepsilon U}{A}\,, \qquad r = \varepsilon^{-1}(\rho - \rho_0)\,. \tag{5.1}$$

Substituting (5.1) into (1.2), we obtain on $-\infty < r < \infty$ that

$$V'' + \frac{\varepsilon}{\rho_0 + \varepsilon r} V' - V + V^2 U = 0\,, \tag{5.2a}$$

$$U'' + \frac{\varepsilon}{\rho_0 + \varepsilon r} U' - \varepsilon^2 U + A\varepsilon - V^2 U = 0\,. \tag{5.2b}$$

Therefore, we expand V and U in a powers of εA as in (2.3) to get that U_0, V_0 satisfy (2.4), and that U_1, V_1 satisfy

$$V_1'' - V_1 + 2V_0 U_0 V_1 + V_0^2 U_1 = -\frac{V_0'}{A\rho_0}\,, \tag{5.3a}$$

$$U_1'' + 1 - 2V_0 U_0 V_1 - V_0^2 U_1 = -\frac{U_0'}{A\rho_0}\,. \tag{5.3b}$$

The asymptotic boundary conditions for U_1 as $r \to \pm\infty$ are to be obtained by matching.

Next, we consider the outer region defined away from ρ_0. By calculating uv^2 in the sense of distributions as in (2.6) of §2, we obtain, in place of (2.7), the following outer problem for $u(\rho)$:

$$u_{\rho\rho} + \frac{1}{\rho} u_\rho + 1 - u = C_0 \delta(\rho - \rho_0) + \varepsilon C_1 \delta(\rho - \rho_0) + \cdots , \quad 0 < \rho < R ; \qquad u_\rho(R) = u_\rho(0) = 0 . \quad (5.4)$$

Here C_0 and C_1 are defined in (2.6) of §2. Therefore, we obtain the two-term outer expansion

$$u = 1 - C_0 G(\rho; \rho_0) - \varepsilon C_1 G(\rho; \rho_0) + \cdots , \quad (5.5)$$

where $G(\rho; \rho_0)$ is the radially symmetric Green's function satisfying

$$G_{\rho\rho} + \frac{1}{\rho} G_\rho - G = -\delta(\rho - \rho_0) , \quad 0 < \rho < R ; \qquad G_\rho(R; \rho_0) = G_\rho(0; \rho_0) = 0 . \quad (5.6)$$

A simple calculation yields that

$$G(\rho, \rho_0) = \frac{1}{\mathcal{W}(J_2, J_1)} \begin{cases} J_1(\rho) J_2(\rho_0) , & \text{for} \quad 0 < \rho < \rho_0 , \\ J_1(\rho_0) J_2(\rho) , & \text{for} \quad \rho_0 < \rho < R , \end{cases} \quad (5.7a)$$

where $J_1(\rho)$ and $J_2(\rho)$ are defined by

$$J_1(\rho) \equiv I_0(\rho) , \qquad J_2(\rho) \equiv K_0(\rho) - \frac{K_0'(R)}{I_0'(R)} I_0(\rho) . \quad (5.7b)$$

Here I_0 and K_0 are the modified Bessel functions of order zero. In (5.7a), $\mathcal{W}(J_2, J_1)$ is the Wronskian of $J_1(\rho)$ and $J_2(\rho)$ at $\rho = \rho_0$, which we can calculate as

$$\mathcal{W}(J_2, J_1) \equiv J_1'(\rho_0) J_2(\rho_0) - J_1(\rho_0) J_2'(\rho_0) = \frac{1}{\rho_0} . \quad (5.7c)$$

Therefore, from (5.7a), we get that

$$G(\rho_0, \rho_0) = \rho_0 J_1(\rho_0) J_2(\rho_0) . \quad (5.7d)$$

The matching condition between the inner and outer solution is that

$$\begin{aligned} \frac{\varepsilon}{A} \left(U_0(r) + A\varepsilon U_1(r) + \cdots \right) \sim 1 - C_0 G(\rho_0, \rho_0) - \left(C_0 G_\rho(\rho_0^\pm; \rho_0) r + C_1 G(\rho_0; \rho_0) \right) \varepsilon \\ - \left(\frac{r^2}{2} C_0 G_{\rho\rho}(\rho_0^\pm; \rho_0) + C_1 r G_\rho(\rho_0^\pm; \rho_0) \right) \varepsilon^2 + \cdots . \end{aligned} \quad (5.8)$$

The leading-order matching condition yields $1 = C_0 G(\rho_0; \rho_0)$. Using (2.6), this yields that

$$B \equiv \int_0^\infty U_0 V_0^2 \, dr = \frac{A}{2G(\rho_0; \rho_0)} \,. \tag{5.9}$$

From (5.8) we obtain the far-field condition for U_0

$$U_0 \sim -\frac{A G_\rho(\rho_0^\pm; \rho_0)}{G(\rho_0; \rho_0)} r \,, \quad \text{as} \quad r \to \pm\infty \,. \tag{5.10}$$

The equilibrium ring location ρ_0 is such that U_0 and V_0 are even functions (cf. [15]). This requirement is readily seen by applying a solvability condition to (5.3). This condition yields that $U_0'(+\infty) + U_0'(-\infty) = 0$, so that $G_\rho(\rho_0^+, \rho_0) = -G_\rho(\rho_0^-, \rho_0)$ from (5.10). Therefore, ρ_0 satisfies the following transcendental equation:

$$\left[J_1(\rho) J_2(\rho)\right]' |_{\rho=\rho_0} = 0 \,. \tag{5.11}$$

It was shown in Lemma 3.4 of [15] that there is a root ρ_0, with $0 < \rho_0 < R$, to (5.11).

Since, in addition, $G_\rho(\rho_0^+, \rho_0) - G_\rho(\rho_0^-, \rho_0) = -1$, we get that $G_\rho(\rho_0^\pm; \rho_0) = \mp 1/2$. Therefore, from (5.10), U_0 has the asymptotic behavior $U_0 \sim B|r|$ as $r \to \pm\infty$, where B is given in (5.9). Therefore, U_0 and V_0 satisfy the same core problem as in §2. A two-term far-field expansion for U_0 is then given in (2.13). Substituting (2.13) into (5.8), we obtain the far-field form for U_1 given by

$$U_1 \sim -\frac{r^2}{2} - \frac{Er}{4[G(\rho_0; \rho_0)]^2} + \cdots \,, \qquad \text{as} \quad r \to \pm\infty \,, \tag{5.12}$$

where E is defined in (2.13).

This leads to the following result for the equilibrium ring radius ρ_0:

Proposition 8 *(cf. [15]). Let $\Omega = \{x : |x| \equiv \rho < R\}$, and*

$$B = \frac{A}{2G(\rho_0; \rho_0)} = \frac{A}{2\rho_0 J_1(\rho_0) J_2(\rho_0)} \,. \tag{5.13}$$

Here ρ_0 is the root of (5.11), where J_1 and J_2 are defined in (5.7b). Suppose that $A = O(1)$ and $B < 1.347$. Then, along the primary branch of the γ versus B curve associated with the core problem of §2, there exists an equilibrium ring solution to (1.2) of the form

$$v_e \sim \frac{1}{\varepsilon} \left(V_0(r) + \cdots\right) \qquad u_e \sim \frac{\varepsilon}{A} \left(U_0(r) + \cdots\right) \,, \qquad r = \varepsilon^{-1}(\rho - \rho_0) \,, \tag{5.14}$$

where $V_0(y)$, $U_0(y)$ are even solutions to (2.4) subject to $V_0 \to 0$ and $U_0' \to B$ as $r \to +\infty$. In the outer region, v_e is exponentially small, and the leading-order approximation to u_e is

$$u_e \sim 1 - \frac{G(\rho; \rho_0)}{G(\rho_0; \rho_0)} + O(\varepsilon) \,, \tag{5.15}$$

where G is the Green's function given in (5.7).

Next, we analyze zigzag instabilities associated with an equilibrium ring solution. We introduce a perturbation around the equilibrium state in the form

$$v = v_e + e^{\lambda t} e^{im\theta} \phi \,, \qquad u = u_e + e^{\lambda t} e^{im\theta} \eta \,, \qquad . \tag{5.16}$$

where $\phi \ll 1$, $\eta \ll 1$, and m is a non-negative integer. Substituting (5.16) into (1.2), we obtain, in place of (3.3), the following eigenvalue problem on $0 < \rho < R$:

$$\lambda \phi = \varepsilon^2 \left(\phi_{\rho\rho} + \frac{1}{\rho} \phi_\rho \right) - \frac{\varepsilon^2 m^2}{\rho^2} \phi - \phi + 2 A u_e v_e \phi + A v_e^2 \eta \,, \tag{5.17a}$$

$$\tau \lambda \eta = \eta_{\rho\rho} + \frac{1}{\rho} \eta_\rho - \frac{m^2}{\rho^2} \eta - \eta - 2 u_e v_e \phi - v_e^2 \eta \,. \tag{5.17b}$$

We will study this problem in the inner region where $r = \varepsilon^{-1}(\rho - \rho_0) = O(1)$, and in the outer region where $\rho - \rho_0 = O(1)$.

In the inner region, we write

$$u_e = \frac{\varepsilon}{A} U \,, \quad v_e = \frac{V}{\varepsilon} \,, \quad \phi = \frac{1}{\varepsilon} \Phi \,, \quad \eta = \frac{\varepsilon}{A} N \,, \quad r = \varepsilon^{-1} (\rho - \rho_0) \,. \tag{5.18}$$

In terms of these variables, (5.17) reduces to an eigenvalue problem on $-\infty < r < \infty$

$$\lambda \Phi = \Phi'' + \frac{\varepsilon}{\rho_0 + \varepsilon r} \Phi' - \frac{\varepsilon^2 m^2}{(\rho_0 + \varepsilon r)^2} \Phi - \Phi + V^2 N + 2 V U \Phi \,, \tag{5.19a}$$

$$\tau \varepsilon^2 \lambda N = N'' + \frac{\varepsilon}{\rho_0 + \varepsilon r} N' - \frac{\varepsilon^2 m^2}{(\rho_0 + \varepsilon r)^2} N - \varepsilon^2 N - V^2 N - 2 V U \Phi \,. \tag{5.19b}$$

We first assume that $m = O(1)$ as $\varepsilon \to 0$. By expanding V, U, Φ, and N, in powers of εA, and writing $\lambda = \varepsilon A \lambda_0$, we derive (3.7) for Φ_0 and N_0. Thus, $\Phi_0 = V_0'$ and $N_0 = U_0'$. The system for Φ_1 and N_1 is (3.8), with the terms $-\Phi_0'/(A\rho_0)$ and $-N_0'/(A\rho_0)$ added to the right-hand sides of (3.8a) and (3.8b), respectively. Since these additional terms are even functions, they do not contribute to the solvability condition that determines λ_0. Therefore, the entire analysis of (3.10)–(3.15) can be repeated, and we obtain that λ_0 satisfies

$$\lambda_0 = -\alpha \left(\frac{N_1'(+\infty) + N_1'(-\infty)}{2} + 1 \right) \,, \qquad \alpha \equiv \frac{-\Psi_2^\dagger(+\infty)}{\int_0^\infty \Psi_1^\dagger V_0' \, dy} \,. \tag{5.20}$$

Here $\Psi_j^\dagger$ for $j = 1, 2$ is the solution to the adjoint problem (3.11).

To determine $N_1'(\pm\infty)$ we must consider the outer region. By repeating the analysis of (3.18)–(3.19), we obtain that the outer solution for η on $0 < \rho < R$ satisfies

$$\eta_{\rho\rho} + \frac{1}{\rho} \eta_\rho - \frac{m^2}{\rho^2} \eta - (1 + \tau\lambda) \eta = \frac{2B\varepsilon}{A} \delta'(\rho - \rho_0) + \varepsilon \left[N_1'(+\infty) - N_1'(-\infty) \right] \delta(\rho - \rho_0) \,, \tag{5.21}$$

with $\eta_\rho(R)=0$ and $\eta_\rho(0)=0$. The matching condition of the inner and outer solutions for η is

$$\frac{\varepsilon}{A}\left(N_0+\varepsilon A N_1+\cdots\right)\sim \eta\left(\rho_0^{\pm}\right)+\varepsilon r \eta_\rho\left(\rho_0^{\pm}\right)+\cdots . \tag{5.22}$$

Since $N_0=U_0^{'}$ satisfies $N_0(\pm\infty)=\pm B$, we get from this matching condition that

$$\eta\left(\rho_0^{\pm}\right)=\pm\frac{\varepsilon B}{A}=\pm\frac{\varepsilon}{2G(\rho_0;\rho_0)}\,, \qquad N_1^{'}(\pm\infty)=\varepsilon^{-1}\eta_\rho\left(\rho_0^{\pm}\right) . \tag{5.23}$$

Solving (5.21) for $\eta(\rho)$, we obtain that

$$\eta(\rho)=\begin{cases} \eta\left(\rho_0^{+}\right) J_{2,m}(\rho)/J_{2,m}(\rho_0)\,, & \rho<\rho_0<R\,,\\ \eta\left(\rho_0^{-}\right) J_{1,m}(\rho)/J_{1,m}(\rho_0)\,, & 0<\rho<\rho_0\,. \end{cases}$$

Here $J_{1,m}$ and $J_{2,m}$ are defined by

$$J_{2,m}(\rho)\equiv K_m(\theta\rho)-\frac{K_m^{'}(\theta R)}{I_m^{'}(\theta R)}I_m(\theta\rho)\,, \qquad J_{1,m}(\rho)\equiv I_m(\theta\rho)\,, \tag{5.24}$$

where I_m, K_m are modified Bessel's functions of the second kind of order m. The constant θ is defined by $\theta\equiv\sqrt{1+\tau\lambda}$. Using (5.23) and the Wronskian relation

$$J_{1,m}'(\rho_0)J_{2,m}(\rho_0)-J_{1,m}(\rho_0)J_{2,m}'(\rho_0)=\frac{1}{\rho_0}\,,$$

we obtain the compact formula

$$\frac{N_1'(+\infty)+N_1'(-\infty)}{2}=-\frac{1}{4\rho_0^2 J_1(\rho_0)J_2(\rho_0)J_{1,m}(\rho_0)J_{2,m}(\rho_0)}\,. \tag{5.25}$$

Substituting (5.25) into (5.20), and recalling that $\lambda\sim\varepsilon A\lambda_0$, we obtain the following result for λ:

Proposition 9 *Consider an equilibrium ring solution of radius ρ_0 for the Gray-Scott model in a disk of radius R as constructed in Proposition 8. Suppose that $m=O(1)$ as $\varepsilon\to 0$. Then, for a perturbation of the form (5.16), λ satisfies the transcendental equation*

$$\lambda\sim-\varepsilon A\alpha\left(1-\frac{1}{4\rho_0^2 J_1(\rho_0)J_2(\rho_0)J_{1,m}(\rho_0)J_{2,m}(\rho_0)}\right)\,. \tag{5.26}$$

As shown in §2, the constant α, defined in (3.25), is positive along the primary branch of the γ versus B curve. It depends only on B and was plotted in Fig. 2. The functions J_1, J_2 are defined in (5.7b). Finally, the functions $J_{1,m}$, $J_{2,m}$, which were defined in (5.24), depend on λ through the parameter θ given by

$$\theta=\sqrt{1+\lambda\tau}\,, \tag{5.27}$$

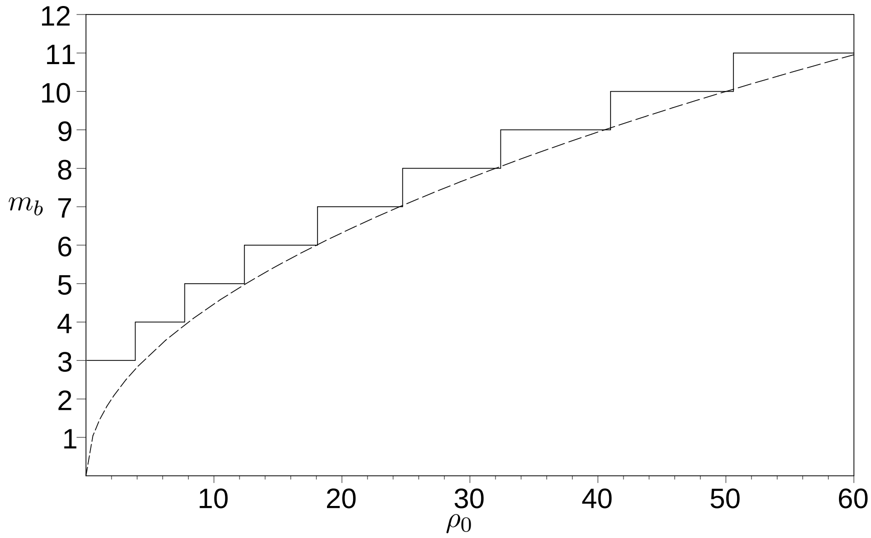

Figure 6: The graph of the first unstable mode m_b versus the ring radius ρ_0 when $\tau = O(1)$. The dotted line is the asymptotic curve (5.32).

We will only consider the case where $\tau = O(1)$ as $\varepsilon \to 0$. Since $\lambda = O(\varepsilon)$, we get $\theta \sim 1$. Therefore, from (5.26) we conclude that λ is positive, and hence we have a zigzag instability, if and only if

$$4\rho_0^2 J_1(\rho_0) J_2(\rho_0) J_{1,m}(\rho_0) J_{2,m}(\rho_0) < 1\,. \tag{5.28}$$

Using the asymptotic expansion for large m and fixed R, it is easy to show that $J_{1,m}J_{2,m} = O(\frac{1}{m})$ for $m \gg 1$ and ρ_0 fixed (see below). Therefore, from (5.28), we have an instability if m is large enough. In Fig. 6 we show the numerical computation of the first unstable mode $m = m_b$ versus the ring radius ρ_0. The corresponding disk radius R can be determined in terms of ρ_0 from (5.11). From this figure we notice that the first two modes $m = 1, 2$ are stable for any ρ_0. Also note that the first unstable mode increases as the ring radius ρ_0 is increased. This is in contrast to the result for stripes in §3, where the first unstable mode tends to zero as the domain half-length l is increased.

We cannot analytically determine m_b for arbitrary R. However, by considering the two limiting cases $R \ll 1$ and $R \gg 1$, we can obtain the following limit results:

Proposition 10 *The following asymptotic formulae relate the domain radius R and the equilibrium* *ring radius ρ_0, as defined by the solution to (5.11):*

$$R \sim \sqrt{2}\rho_0\,, \qquad R \to 0\,, \tag{5.29}$$

$$R \sim \rho_0 + \frac{1}{2}\ln(2\rho_0)\,, \qquad R \to \infty\,. \tag{5.30}$$

Suppose that $\tau = O(1)$, and let m_b be the smallest value of m for which the eigenvalue of Proposition 9 is unstable. Then

$$m_b = 3\,, \qquad R \to 0\,, \tag{5.31}$$

$$m_b \sim \sqrt{2\rho_0}\,, \qquad R \to \infty\,. \tag{5.32}$$

By calculating ρ_0 in terms of R from (5.30), (5.32) can be written as $m \sim \sqrt{2(R - \frac{1}{2}\ln(2R) + \cdots)}$.

We now derive this result. We first consider the case $R \to 0$. A simple calculation using (5.7b) shows that the equilibrium condition (5.11) for ρ_0 can be written as

$$\frac{K_0(\rho_0)}{I_0(\rho_0)} - \frac{K_0'(R)}{I_0'(R)} = \frac{1}{2\rho_0 I_0(\rho_0) I_0'(\rho_0)}\,. \tag{5.33}$$

For $R \to 0$, with $0 < \rho_0 < R$, we use the small argument expansions of I_0 and K_0 to obtain that

$$2\rho_0 I_0(\rho_0) I_0'(\rho_0) \sim \rho_0^2\,, \qquad \frac{K_0'(R)}{I_0'(R)} \sim -2R^{-2}\,, \qquad \frac{K_0(\rho_0)}{I_0(\rho_0)} \sim -\ln\rho\,.$$

Therefore, (5.33) reduces to $2R^{-2} \sim \rho^{-2}$. This yields $R \sim \sqrt{2}\rho_0$, which establishes (5.29).

Next, we determine the stability threshold m_b for $R \to 0$. Using the small argument expansions of I_0 and K_0, we readily obtain that

$$J_1(\rho_0) J_2(\rho_0) \sim \frac{2}{R^2} \sim \rho_0^{-2}\,. \tag{5.34}$$

Using (5.24), and the small argument expansions

$$K_m(\rho_0) \sim \frac{1}{2}\Gamma(m)\left(\frac{\rho_0}{2}\right)^{-m} \qquad I_m(\rho_0) \sim \frac{1}{\Gamma(m+1)}\left(\frac{\rho_0}{2}\right)^{m}\,, \tag{5.35}$$

we calculate for $R \ll 1$ and $\rho \ll 1$ that

$$J_{1,m}(\rho_0) J_{2,m}(\rho_0) = I_m(\rho_0) K_m(\rho_0) - \frac{K_m'(R)}{I_m'(R)} \left(I_m(\rho_0)\right)^2 \sim \frac{1}{2}\frac{\Gamma(m)}{\Gamma(m+1)}\left(1 + \frac{1}{2^m}\right)\,. \tag{5.36}$$

Here $\Gamma(m)$ is the Gamma function. Therefore, substituting (5.34) and (5.36) into (5.28), we have instability when $R \ll 1$ if and only if

$$\frac{m}{1+2^{-m}} - 2 > 0\,. \tag{5.37}$$

The first integer for which (5.37) holds is $m_b = 3$, which establishes (5.31).

Next, we derive the results in Proposition 10 for $R \gg 1$. To do so, we need the following standard asymptotic formulae (cf. [2]):

$$K_0(z) \sim \sqrt{\frac{\pi}{2z}} e^{-z} \left(1 - \frac{1}{8z}\right)\,, \qquad I_0(z) \sim \sqrt{\frac{1}{2\pi z}} e^{z} \left(1 + \frac{1}{8z}\right)\,. \tag{5.38}$$

Therefore, we get

$$\frac{K_0(\rho_0)}{I_0(\rho_0)} \sim \frac{\pi}{e^{2\rho_0}} \left(1 - \frac{1}{4\rho_0}\right)\,, \quad \frac{K_0'(R)}{I_0'(R)} \sim -\frac{\pi}{e^{2R}} \left(1 - \frac{3}{4R}\right)\,, \quad I_0(\rho_0) I_0'(\rho_0) \sim \frac{e^{2\rho_0}}{2\pi\rho_0} \left(1 - \frac{1}{4\rho_0}\right)\,.$$

Substituting these formulae into (5.33), we get that

$$\frac{\pi}{2\rho_0} e^{-2\rho_0} \sim \pi e^{-2R} \left(1 - \frac{3}{4R}\right)\,.$$

Solving this equation asymptotically, we get $R \sim \rho_0 + \frac{1}{2}\ln(2\rho_0)$ as $R \to \infty$, which establishes (5.30).

Finally, we establish the stability threshold (5.32) for $R \gg 1$. Using (5.38) and (5.30), we readily estimate that

$$J_1(\rho_0) J_2(\rho_0) \sim \frac{1}{2}\left(1 + e^{2\rho_0 - 2R}\right) \sim \frac{1}{2\rho_0}\left(1 + \frac{1}{2\rho_0}\right)\,. \tag{5.39}$$

Next, we must calculate $J_{1,m}(\rho_0) J_{2,m}(\rho_0)$. Since, we have $m_b \gg 1$ and $\rho_0 \gg 1$, we must use the following *uniform* expansions of $K_m(mz)$ and $I_m(mz)$ for $m \to \infty$ as given in [2]:

$$K_m(mz) \sim \sqrt{\frac{\pi}{2m}} \frac{e^{-m\beta(z)}}{(1+z^2)^{1/4}}\,, \qquad I_m(mz) \sim \frac{1}{\sqrt{2\pi m}} \frac{e^{m\beta(z)}}{(1+z^2)^{1/4}}\,, \tag{5.40}$$

where $\beta(z)$ is defined by

$$\beta(z) \equiv \sqrt{1+z^2} + \ln z - \ln\left(1 + \sqrt{1+z^2}\right)\,. \tag{5.41}$$

Defining z and z_1 by

$$z = \frac{\rho_0}{m}\,, \qquad z_1 = \frac{R}{m}\,,$$

we get using (5.40) that

$$J_{1,m}(\rho_0) J_{2,m}(\rho_0) \sim \frac{1}{2m\sqrt{1+z^2}} \left(1 + e^{2m[\beta(z) - \beta(z_1)]}\right)\,. \tag{5.42}$$

Since $R = \rho_0 + \frac{1}{2}\ln(2\rho_0)$, we have that $z - z_1 \to 0$ provided that $\ln(\rho_0)/m \ll 1$. Assuming for the moment that this condition is true, we can then use $\beta^{'}(z) = z^{-1}\sqrt{1+z^2}$ to estimate

$$\beta(z) - \beta(z_1) \sim \beta^{'}(z)(z - z_1) \sim -\frac{1}{2mz}\ln(2\rho_0)\sqrt{1+z^2}\,.$$

Substituting this expression into (5.42), and using (5.39), the stability threshold condition defined by $4\rho_0^2 J_1(\rho_0)J_2(\rho_0)J_{1,m}(\rho_0)J_{2,m}(\rho_0) = 1$ becomes

$$\frac{z}{\sqrt{1+z^2}}\left(1 + \frac{1}{2\rho_0}\right)\left(1 + e^{-\ln(2\rho_0)z^{-1}\sqrt{1+z^2}}\right) \sim 1\,, \tag{5.43}$$

where $z \equiv \rho_0/m$. If we assume that $z = O(1)$ and $\rho \gg 1$, then it is easy to see that there is no root to (5.43). Therefore, we must assume that $z \gg 1$. In this limit, (5.43) reduces to

$$\frac{z}{\sqrt{1+z^2}}\left(1 + \frac{1}{2\rho_0}\right)^2 \sim 1\,.$$

Squaring both sides, we readily obtain that $\rho_0 \sim 2z^2$. Since $z = \rho_0/m$, we get that $m = \sqrt{2\rho_0}$, which establishes (5.32). The consistency condition $\ln(2\rho_0)/m \ll 1$ needed above is indeed satisfied.

The results above show that for $m > m_b$ an equilibrium ring solution is unstable due to a zigzag instability. For the other distinguished limit where $m = O(\varepsilon^{-1/2})$, we can use (5.42) to get that $J_{1,m}(\rho_0)J_{2,m}(\rho_0) \sim (2m)^{-1}$ for fixed ρ_0. Using this relation in (5.26), we conclude that $\lambda = O(\varepsilon^{1/2})$ and $\lambda > 0$. However, as was the case in our study in §3 of zigzag instabilities of a stripe equilibrium, the ring re-stabilizes when $m = O(\varepsilon^{-1})$. In this regime, we introduce m_0 by $m = m_0\varepsilon^{-1}$, where $m_0 = O(1)$. From (5.19), we obtain the following leading-order eigenvalue problem defined on $-\infty < r < \infty$:

$$\left(\lambda + \frac{m_0^2}{\rho_0^2}\right)\Phi_0 = \Phi_0'' - \Phi_0 + V_0^2 N_0 + 2V_0U_0\Phi_0\,, \tag{5.44a}$$

$$\frac{m_0^2}{\rho_0^2}N_0 = N_0'' - V_0^2 N_0 - 2V_0U_0\Phi_0\,. \tag{5.44b}$$

We seek an odd eigenfunction to this problem for which $\Phi_0 \to 0$ and $N_0 \to 0$ as $r \to \pm\infty$. This problem is precisely the same eigenvalue problem as (3.39) once we replace m_0 in (3.39) with m_0/ρ_0. Therefore, we obtain the next result:

Proposition 11 *Consider an equilibrium ring solution of radius ρ_0 for the Gray-Scott model in a disk of radius R as constructed in Proposition 8. Then, all zigzag perturbations of the form (5.16) are unstable in the zone $m_b < m < \varepsilon^{-1}\rho_0 m_{0u}$, and are stable outside of this zone. Here m_b is the root of*

$4\rho_0^2 J_1(\rho_0)J_2(\rho_0)J_{1,m}(\rho_0)J_{2,m}(\rho_0) = 1$, which depends on R. The threshold m_{0u}, computed in §3 and plotted in Fig. 4, is independent of R but depends on the value of B along the primary branch of the γ versus B bifurcation diagram.

Finally, the stability property of a ring with respect to a breakup instability is very similar to that of a stripe. Our final result is as follows:

Proposition 12 *Consider an equilibrium ring solution given in Proposition 8, in the intermediate regime $B = 3\delta \ll 1$. Such a solution is unstable with respect to perturbations of the form (5.16), where ϕ and η are now even functions in the inner region, if and only if the following inequality holds:*

$$3\delta^2 \rho_0 < \varepsilon m < \frac{\sqrt{5}}{2}\rho_0 \,. \tag{5.45}$$

In the high feed-rate regime, the instability band is given by

$$\sqrt{\mu_1}\rho_0 < \varepsilon m < \sqrt{\mu_2}\rho_0 \,, \tag{5.46}$$

where $\mu_1 = \mu_1(B)$ and $\mu_2 = \mu_2(B)$ are given in Table 1 and plotted in Fig. 5.

The result (5.46) follows immediately by noting that the eigenvalue problems (4.2) and (5.44) are equivalent if we replace $\mu = \varepsilon^2 m^2$ in (4.2) with $\mu = \varepsilon^2 m^2/\rho_0^2$. The result (5.45) is also readily obtained by a slight modification of the analysis in §4. To obtain (5.45), we repeat the analysis of (4.3)–(4.16). The upper bound in (5.45) follows from (4.4). Then, to determine the lower bound in (5.45), we re-derive the nonlocal eigenvalue problem (4.15), where the multiplier χ in (4.16) is to be replaced with

$$\chi = 2\left[1 + \frac{\varepsilon\delta^{-2}}{6G_m(\rho_0;\rho_0)}\right]^{-1}, \qquad G_m(\rho_0;\rho_0) \equiv \rho_0 J_{1,m}(\rho_0)J_{2,m}(\rho_0) \,. \tag{5.47}$$

Here $G_m(\rho_0;\rho_0)$ is the Green's function, evaluated at $\rho = \rho_0$, for the operator $\eta'' + \rho^{-1}\eta' - m^2\rho^{-2}\eta = -\delta(\rho - \rho_0)$ with $\eta'(0) = \eta'(R) = 0$. In (5.47), $J_{1,m}$ and $J_{2,m}$ are defined in (5.24). From Lemma 6, the stability threshold occurs when $\chi = 1$. Since $\varepsilon\delta^{-2} \ll 1$ in the intermediate regime where $\delta \gg O(\varepsilon^{1/2})$, we conclude that all modes with $m = O(1)$ are stable. However, since $J_{1,m}J_{2,m} \sim (2m)^{-1}$ as $m \to \infty$ for fixed ρ_0, we have that χ will decrease below unity when m is below the lower bound in (5.45).

6 Numerical Examples

In this section we give a few numerical examples to partially confirm our analytical results for zigzag and breakup instabilities. All of the numerical computations for (1.2) have been done with the software package "VLUGR" [3].

Example 1: Zigzag Instability of a Stripe: In order to observe zigzag instabilities, one must choose parameters and initial conditions carefully so that these instabilities are not dominated by breakup instabilities that occur on shorter timescales. In this example, we consider a stripe equilibrium with $\varepsilon = 0.004$, $A = 1.7$, and $\tau = 1.0$, in the rectangular domain $[-1, 1] \times [0, 1]$ so that $d = l = 1$. For this value of A, we compute that $B = A \tanh 1 = 1.3 < 1.35$. Hence, by Proposition 1, there is a stripe equilibrium solution centered along $x_1 = 0$. For these parameter values, we obtain from Proposition 5 that the unstable modes m satisfy $m_b < m < m_{0u}/\varepsilon$, where $m_b \approx 1.05$ when $l = 1$, and $m_{0u} \approx 0.72$ when $B = 1.3$. This yields the instability zone $1.05 < m < 180$ when $\varepsilon = .004$.

The meshsize in the x_1 direction must be finer than ε in order to resolve the stripe. With $\varepsilon = 0.004$, the computation would be quite prohibitive for most uniform-grid codes. Fortunately, VLUGR uses an adaptive mesh-refinement algorithm, which captures the localized structure of the stripe without the need for a huge number of grid points.

For the initial conditions for (1.2) we took $v = \frac{1}{\varepsilon} w\left(\frac{x_1 + 10^{-4}\cos(10\pi x_2)}{\varepsilon}\right)$ and $u = \varepsilon$, where $w(y) = \frac{3}{2}\text{sech}^2(y/2)$ satisfies (2.22). Therefore, the preference for a zigzag instability corresponding to the mode $m = 10\pi$, which lies within the instability zone, is built in. The resulting numerical simulation is shown in Fig. 7. The system does indeed develop a zigzag instability corresponding to this mode.

Numerically, we can also validate the theoretically predicted form of the zigzag instability. From the theory of §3, we would expect that the eigenfunction ϕ has the form

$$\phi = \frac{d}{dx_1} v_e(x_1) \cos mx_2 \,, \tag{6.1}$$

where v_e is the equilibrium stripe. Since $v \sim v_e + Ce^{\lambda t}\phi$ and $\lambda = O(\varepsilon) \ll 1$, we have that ϕ is well-approximated by the difference in the numerical solution at two different times. From results obtained from our numerical simulations, we plot $v_{t=22} - v_{t=18}$ in Fig. 8. From this figure we observe that the shape of the resulting perturbation is indeed of the form (3.9).

The onset of a breakup instability for this example is visible in Fig. 7 at time $t = 32$, when the wiggled stripe starts to develop an instability. Shortly after this time, the stripe breaks up into spots, which then self-replicate until the entire rectangle is full of spots.

Example 2: Breakup Instability of a Stripe: Next, we verify Proposition 7 for the parameter set $\varepsilon = 0.004$, $A = 1.313$, $l = 1$, and $d = 2$. For this value of A, we compute that $B = A\tanh(1) = 1$. From Table 1, we have have $\mu_1 = 0.0659, \mu_2 = 0.9208$. Therefore, from Proposition 7, the instability

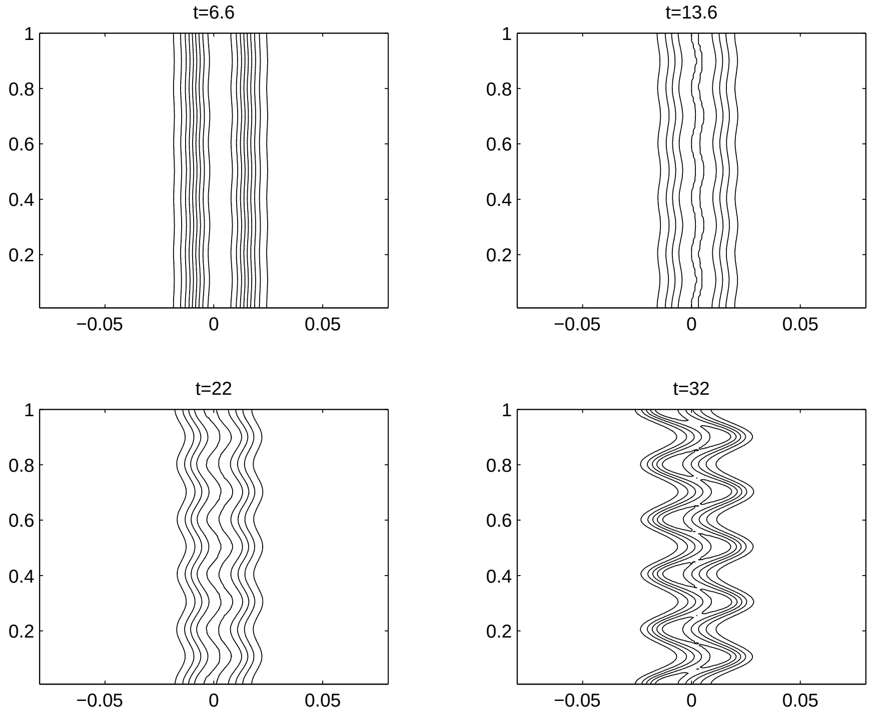

Figure 7: Contour plot of v obtained from the full numerical solution of (1.2). The parameters are $\varepsilon = 0.004$, $A = 1.7$, $\tau = 1.0$, and the domain size was set to $[-1, 1] \times [0, 1]$. The initial condition was taken to be $v = \frac{1}{\varepsilon} w\left(\frac{x_1 + 10^{-4}\cos(2\pi 5 x_2)}{\varepsilon}\right)$, $u = \varepsilon$, where $w(y) = \frac{3}{2}\text{sech}^2(y/2)$. Outside the region shown, v is exponentially small.

zone is $64.2 \leq m \leq 239.9$. To check this, we start with the following initial condition for v that has a built-in preference for the the mode $m = 20\pi = 62.8$:

$$v = \frac{1}{\varepsilon}(1 + 10^{-4}\cos(20\pi x_2)) w\left(\frac{x_1}{\varepsilon}\right), \qquad u = \varepsilon, \tag{6.2}$$

where $w(y) = \frac{3}{2}\text{sech}^2(y/2)$ is given by (2.22). Note that this mode is *stable*. Indeed, in the resulting simulation shown in Fig. 9, the stripe breaks up into 21 and not 20 spots. This corresponds to $m = 21\pi = 66$, which lies just within the theoretical instability band.

Example 3: Space-Filling Curve: In this example, we numerically show the development of a zigzag instability in the weak interaction regime, where both u and v are localized near $x_1 = 0$. For convenience, we introduce an extra parameter D to be the diffusivity coefficient of u. In this way,

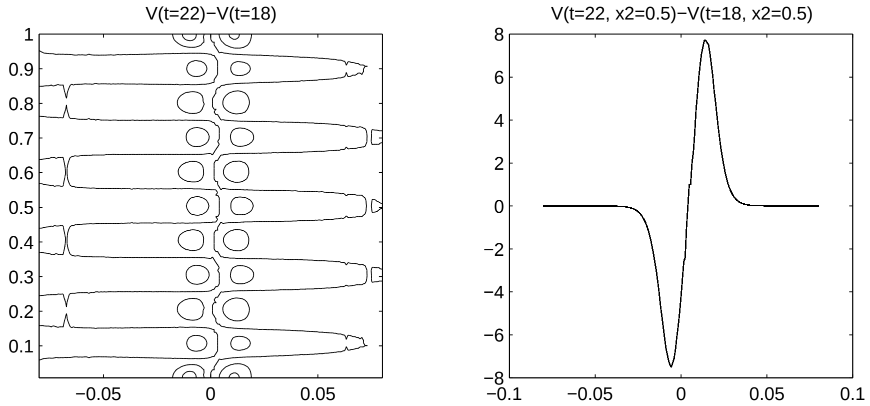

Figure 8: Left: contour plot of $v_{t=22} - v_{t=18}$ for the data of Fig. 7. Right: The horizontal slice of the figure on the left at $x_2 = 0.5$.

(1.2) is replaced by

$$\begin{cases} v_t = \tilde{\varepsilon}^2 \triangle v - v + A v^2 u \,, \\ \tau u_t = D \triangle u - u + 1 - v^2 u \,. \end{cases} \tag{6.3}$$

For this computation we take $\tilde{\varepsilon} = 0.05$, $D = 0.01$, $A = 2.0$, $l = 1$, and $d = 5$. This corresponds to the weak interaction regime, whereby both u and v are localized near the stripe, and is similar to parameter regimes studied in [23], [24], and [28]. Notice that by re-scaling, these parameter values are equivalent to taking $\varepsilon = 0.5$ $D = 1$, $l = 10$, and $d = 50$, in (1.2). Therefore, since ε is rather large, the theoretical analysis of §3 and §4 is not applicable. The numerical results are shown in Fig. 10 and Fig. 11. The zigzag instability corresponding to the mode $\cos\left(\frac{3}{2\pi 5} x_2\right)$ becomes unstable and, in contrast to Example 2, we do not observe any instabilities that lead to the development of spots. The end state seems to be a domain-filling curve. We ran the simulation to about $t = 10000$; the solution seems to have reached a steady state at this time, since no changes in the solution were observed between $t = 8000$ and $t = 10000$.

Example 4: Zigzag Instability of a Ring: In this example, we consider (6.3) and we take the parameter values $\tilde{\varepsilon} = 0.05$, $D = 0.01$, $A = 2.0$, in a rectangular domain $\Omega = [-2, 2] \times [0, 4]$, so that $l = 2$ and $d = 4$. Since this parameter set again corresponds to the weak interaction regime, it is not in the scope of our theoretical analysis. We take the initial condition to be a spot at the center of the domain. After a short time, the spot grows into an expanding ring. Some time later, this ring develops a zigzag instability corresponding to the mode $m = 4$. The end state of this computation is again a complicated domain-filling curve as shown in Fig. 12. In [19], similar zigzag instabilities of a ring have been observed in the weak interaction regime.

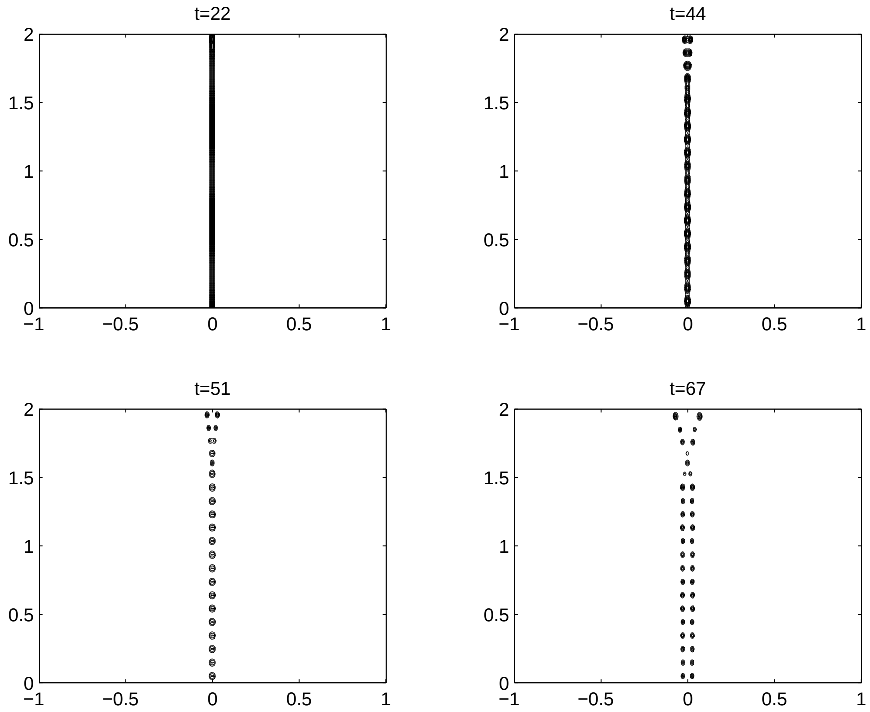

Figure 9: Contour plot of v computed from the full numerical simulation of (1.2). The domain size was set to $[-1,1] \times [0,1]$, and the parameter values are $\varepsilon = 0.004$, $A = 1.313$, and $\tau = 1.0$. The initial condition was taken to be (6.2).

7 Discussion

We have analyzed zigzag and breakup instabilities of stripes and rings for the Gray-Scott model (1.2) in the semi-strong interaction regime where v is localized and where the variation of u occurs over the extent of the domain. In this semi-strong interaction regime we have found that there is an instability band for both types of instabilities. The instability bands have been determined for both the high feed-rate regime where $A = O(1)$, and for the intermediate regime where $O(\varepsilon^{1/2}) \ll A \ll O(1)$.

A natural extension of this work is to determine whether there is a parameter regime where the instability bands disappear. One way to stabilize a stripe is to take the domain width d to be very small. Indeed, since the upper bound of the instability band is $O(\varepsilon^{-1})$, a stripe can be stable if we take the domain width to be of order $O(\varepsilon)$. Such an analysis was performed in [6]. A different possibility is to analyze zigzag and breakup instabilities of a stripe and ring solution in the weak interaction regime of [23], [24], [28], and [12], where u and v are both exponentially localized near a stripe or a ring. This

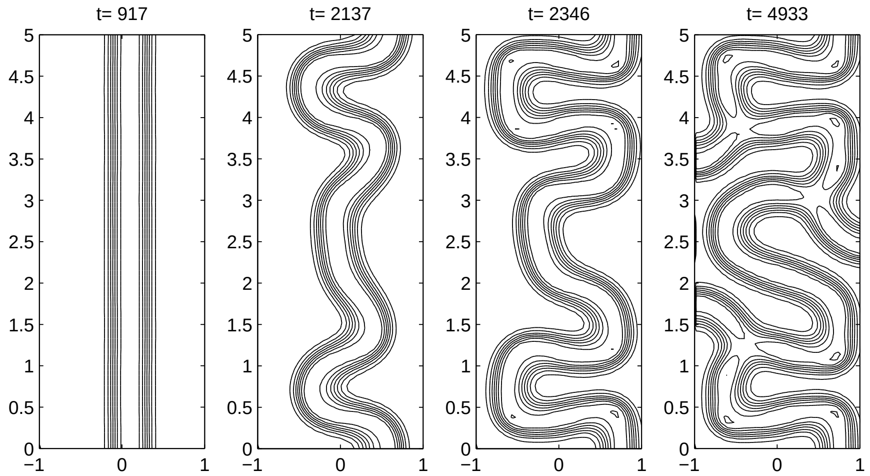

Figure 10: Contour plot of v for Example 3 at the times indicated.

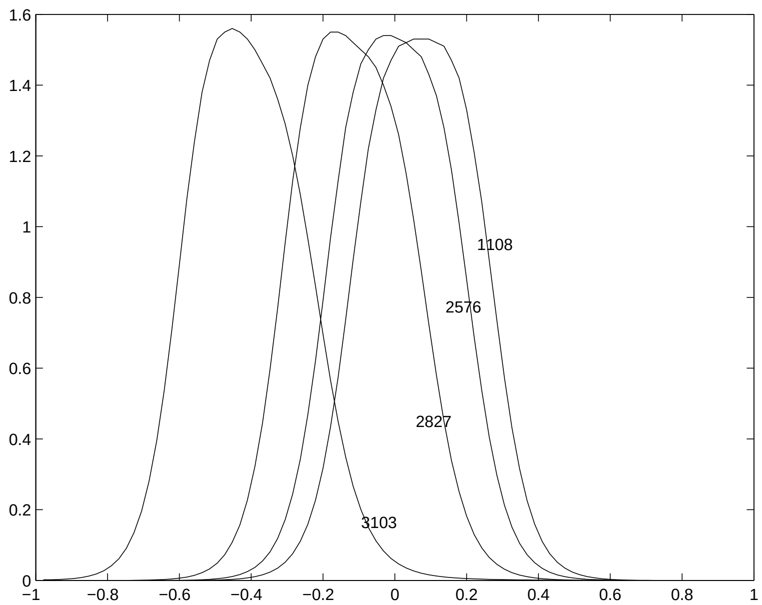

Figure 11: Plots of $v(x_1, x_2)$ versus x_1 with $x_2 = 2.5$.

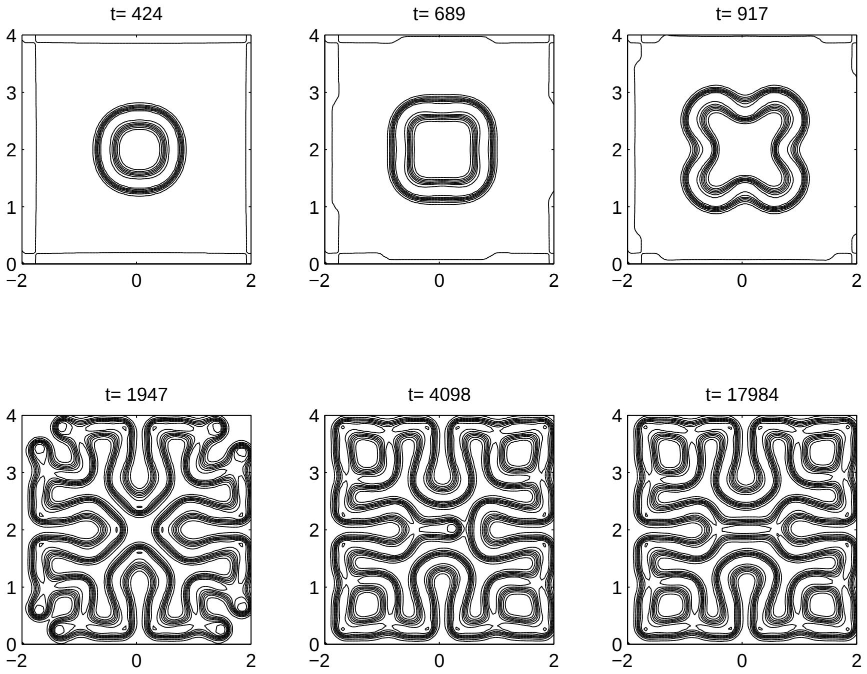

Figure 12: Contour plot of v for Example 4 showing the zigzag instability of a ring and the labyrinthine pattern that results at later time.

regime corresponds to taking $D_v = O(D_u) \ll 1$ in (1.1). The numerical computations of Examples 3 and 4 of §6 indicate that there exists values of $D \equiv D_v/D_u = O(1)$, with $D_v = O(D_u) \ll 1$, so that a stripe or ring is stable with respect to breakup instabilities, but is unstable with respect to zigzag instabilities. We conjecture that in the absence of such breakup instabilities a zigzag instability leads to a labyrinthine pattern such as shown in Section 6. An open problem is to study zigzag and breakup instabilities of stripes and rings for the Gray-Scott model in the weak interaction regime.

Acknowledgments. T.K. is supported by a PGS-B graduate scholarship from NSERC Canada. M.J.W. thanks the grant support of NSERC. J.W. is supported by an Earmarked Grant from RGC of Hong Kong. We would like to thank David Iron for his help with setting up the VLUGR code.

References

[1] E. Anderson et al. *LAPACK User's Guide: Third Edition*, SIAM Publications (1999).

[2] M. Abramowitz, I. A. Stegun, *Handbook of Mathematical Functions with Formulas, Graphs, and Mathematical Tables*, Washington, National Bureau of Standards Applied Mathematics, 1964.

[3] J. G. Bom, R. A. Trompert, J. G. Verwer, *Algorithm 758: VLUGR2: A Vectorizable Adaptive Grid Solver for PDEs in 2D*, Association for Computing Machinery Transactions on Mathematical Software, **22**, (1996), pp. 302-328.

[4] A. Doelman, R. A. Gardner, T. J. Kaper, *Stability Analysis of Singular Patterns in the 1D Gray-Scott Model: A Matched Asymptotics Approach*, Physica D, **122**, No. 1-4, (1998), pp. 1-36.

[5] A. Doelman, T. J. Kaper, P. Zegeling, *Pattern Formation in the One-Dimensional Gray-Scott Model*, Nonlinearity, **10**, No. 2, (1997), pp. 523-563.

[6] A. Doelman, H. van der Ploeg, *Homoclinic Stripe Patterns*, SIAM J. Appl. Dyn. Systems, **1**, No. 1, (2002), pp. 65-104.

[7] R. E. Goldstein, D. J. Muraki, D. M. Petrich, *Interface Proliferation and the Growth of Labyrinths in a Reaction-Diffusion System*, Phys. Rev. E., **53**, (1996), pp. 3933-3957.

[8] P. Gray, S. K. Scott, *Autocatalytic Reactions in the Isothermal, Continuous Stirred Tank Reactor: Isolas and Other Forms of Multistability*, Chem. Eng. Sci., **38**, (1983), pp. 29-43.

[9] P. Gray, S. K. Scott, *Autocatalytic Reactions in the Isothermal, Continuous Stirred Tank Reactor: Oscillations and Instabilities in the System $A + 2B \rightarrow 3B$, $B \rightarrow C$*, Chem. Eng. Sci., **39**, (1984), pp. 1087-1097.

[10] A. Hagberg, E. Meron, T. Passot, *Phase Dynamics of Nearly Stationary Patterns in Activator-Inhibitor Systems*, Phys. Rev. E., **61**, No. 6, (2000), pp. 6471-6476.

[11] P. Hirschberg, E. Knobloch, *Zigzag and Varicose Instabilities of a Localized Stripe Pattern*, Chaos, **3**, (1993), pp. 713-721.

[12] J. K. Hale, L. A. Peletier, W. C. Troy, *Exact Homoclinic and Heteroclinic Solutions of the Gray-Scott Model for Autocatalysis*, SIAM J. Appl. Math., **61**, (2000), pp. 102-130.

[13] T. Kolokolnikov, M. Ward, J. Wei, *The Existence and Stability of Spike Equilibria in the One-Dimensional Gray-Scott Model: The Pulse-Splitting Regime*, submitted, Physica D., (2003).

[14] T. Kolokolnikov, M. Ward, J. Wei, *The Existence and Stability of Spike Equilibria in the One-Dimensional Gray-Scott Model: The Low Feed-Rate Regime*, submitted, AMS Monographs, (2003).

[15] T. Kolokolnikov, J. Wei, *On Ring-Like Solutions for the Gray-Scott Model: Existence, Instability, and Self-Replicating Regimes*, submitted, Nonlinearity, (2003).

[16] K. J. Lee, W. D. McCormick, J. E. Pearson, H. L. Swinney, *Experimental Observation of Self-Replicating Spots in a Reaction-Diffusion System*, Nature, **369**, (1994), pp. 215-218.

[17] K. J. Lee, W. D. McCormick, Q. Ouyang, H. L. Swinney, *Pattern Formation by Interacting Chemical Fronts*, Science, **261**, (1993), pp. 192-194.

[18] C. S. Lin, W. M. Ni, I. Takagi, *Large Amplitude Stationary Solutions to a Chemotaxis System*, J. Diff. Eq., **72**, (1988), pp. 1-27.

[19] D. Morgan, T. Kaper, *Axisymmetric Ring Solutions of the Gray-Scott Model and Their Destabilization into Spots*, submitted, Physica D, (2003).

[20] C. Muratov, V. V. Osipov, *Static Spike Autosolitons in the Gray-Scott Model*, J. Phys. A: Math Gen. **33**, (2000), pp. 8893-8916.

[21] C. Muratov, V. V. Osipov, *Stability of the Static Spike Autosolitons in the Gray-Scott Model*, SIAM J. Appl. Math., **62**, No. 5, (2002), pp. 1463-1487.

[22] C. Muratov, V. V. Osipov, *Spike Autosolitons and Pattern Formation Scenarios in the Two-Dimensional Gray-Scott Model*, Eur. Phys. J. B, **22**, (2001), pp. 213-221.

[23] Y. Nishiura, D. Ueyama, *A Skeleton Structure of Self-Replicating Dynamics*, Physica D, **130**, No. 1-2, (1999), pp. 73-104.

[24] Y. Nishiura, D. Ueyama, *Spatio-Temporal Chaos for the Gray-Scott Model*, Physica D, **150**, No. 3-4, (2001), pp. 137-162.

[25] J. E. Pearson, *Complex Patterns in a Simple System*, Science, **216**, (1993), pp. 189-192.

[26] W. N. Reynolds, S. Ponce-Dawson, J. E. Pearson, *Dynamics of Self-Replicating Patterns in Reaction-Diffusion Systems*, Phys. Rev. Lett., **72**, (1994), pp. 2797-2800.

[27] W. N. Reynolds, S. Ponce-Dawson, J. E. Pearson, *Dynamics of Self-Replicating Spots in Reaction-Diffusion Systems*, Phys. Rev. E, **56**, No. 1, (1997), pp. 185-198.

[28] D. Ueyama, *Dynamics of Self-Replicating Patterns in the One-Dimensional Gray-Scott Model*, Hokkaido Math J., **28**, No. 1, (1999), pp. 175-210.

[29] J. Wei, *On Single Interior Spike Solutions for the Gierer-Meinhardt System: Uniqueness and Stability Estimates*, Europ. J. Appl. Math., **10**, No. 4, (1999), pp. 353-378.

[30] J. Wei, *Existence, Stability and Metastability of Point Condensation Patterns Generated by the Gray-Scott System*, Nonlinearity, **12**, (1999), pp. 593-616.

[31] J. Wei, *Pattern Formations in Two-Dimensional Gray-Scott Model: Existence of Single-Spot Solutions and Their Stability*, Physica D, **148**, (2001), pp. 20-48.

[32] J. Wei, M. Winter, *Asymmetric Spotty Patterns for the Gray-Scott Model in R^2*, *Stud. Appl. Math.*, **110**, No. 1, (2003), pp. 63-102.

[33] A. Yochelis, A. Hagberg, E. Meron, A. Lin, H. Swinney, *Development of Standing-Wave Labyrinthine Patterns*, SIAM J. Appl. Dyn. Systems, **1**, No. 2, (2002), pp. 236-247.